Naturalis Repository

Tropical tree mortality has increased with rising atmospheric water stress

David Bauman, Claire Fortunel, Guillaume Delhaye, Yadvinder Malhi, Lucas A. Cernusak, Lisa Patrick Bentley6, Sami W. Rifai7,8, Jesús Aguirre-Gutiérrez2, Imma Oliveras Menor, Oliver L. Phillips, Brandon E. McNellis, Matt Bradford, Susan G. W. Laurance, Michael F. Hutchinson, Raymond Dempsey, Paul E. Santos-Andrade, Hugo R. Ninantay-Rivera, Jimmy R. Chambi Paucar & Sean M. McMahon

DOI:
https://doi.org/10.1038/s41586-022-04737-7

Downloaded from
Naturalis Repository

Article 25fa Dutch Copyright Act (DCA) - End User Rights

This publication is distributed under the terms of Article 25fa of the Dutch Copyright Act (Auteurswet) with consent from the author. Dutch law entitles the maker of a short scientific work funded either wholly or partially by Dutch public funds to make that work publicly available following a reasonable period after the work was first published, provided that reference is made to the source of the first publication of the work.

This publication is distributed under the Naturalis Biodiversity Center 'Taverne implementation' programme. In this programme, research output of Naturalis researchers and collection managers that complies with the legal requirements of Article 25fa of the Dutch Copyright Act is distributed online and free of barriers in the Naturalis institutional repository. Research output is distributed six months after its first online publication in the original published version and with proper attribution to the source of the original publication.

You are permitted to download and use the publication for personal purposes. All rights remain with the author(s) and copyrights owner(s) of this work. Any use of the publication other than authorized under this license or copyright law is prohibited.

If you believe that digital publication of certain material infringes any of your rights or (privacy) interests, please let the department of Collection Information know, stating your reasons. In case of a legitimate complaint, Collection Information will make the material inaccessible. Please contact us through email: collectie.informatie@naturalis.nl. We will contact you as soon as possible.

Tropical tree mortality has increased with rising atmospheric water stress

https://doi.org/10.1038/s41586-022-04737-7

Received: 10 June 2021

Accepted: 6 April 2022

David Bauman[1,2,3]✉, Claire Fortunel[3], Guillaume Delhaye[2,4], Yadvinder Malhi[2], Lucas A. Cernusak[5], Lisa Patrick Bentley[6], Sami W. Rifai[7,8], Jesús Aguirre-Gutiérrez[2,9], Imma Oliveras Menor[2,3], Oliver L. Phillips[10], Brandon E. McNellis[11], Matt Bradford[12], Susan G. W. Laurance[5], Michael F. Hutchinson[13], Raymond Dempsey[5], Paul E. Santos-Andrade[14], Hugo R. Ninantay-Rivera[14], Jimmy R. Chambi Paucar[14] & Sean M. McMahon[1]

Evidence exists that tree mortality is accelerating in some regions of the tropics[1,2], with profound consequences for the future of the tropical carbon sink and the global anthropogenic carbon budget left to limit peak global warming below 2 °C. However, the mechanisms that may be driving such mortality changes and whether particular species are especially vulnerable remain unclear[3–8]. Here we analyse a 49-year record of tree dynamics from 24 old-growth forest plots encompassing a broad climatic gradient across the Australian moist tropics and find that annual tree mortality risk has, on average, doubled across all plots and species over the last 35 years, indicating a potential halving in life expectancy and carbon residence time. Associated losses in biomass were not offset by gains from growth and recruitment. Plots in less moist local climates presented higher average mortality risk, but local mean climate did not predict the pace of temporal increase in mortality risk. Species varied in the trajectories of their mortality risk, with the highest average risk found nearer to the upper end of the atmospheric vapour pressure deficit niches of species. A long-term increase in vapour pressure deficit was evident across the region, suggesting that thresholds involving atmospheric water stress, driven by global warming, may be a primary cause of increasing tree mortality in moist tropical forests.

Tropical forests are critical to the global carbon cycle, and shifts in their long-term dynamics can influence the pace of climate change. There are indications of slowing carbon accumulation in some tropical forests primarily due to changes in mortality[1,2], but uncertainty remains in the scope, severity and mechanisms that might result in global changes in tropical forest structure and dynamics[3–8]. If the tropical forest carbon sink (estimated at 1.2 Pg C per year for recent decades[9]) declines rapidly to zero, the available anthropogenic emissions ‘carbon budget’ to stay below 1.5 °C declines from 115 Pg C to about 100 Pg C, and to stay below 2 °C, it declines from 347 Pg C to about 310 Pg C (refs. [10–12]). Hence, the causes and future of the mortality for tropical forest trees have important consequences for our prospects to stabilise global climate within safe limits.

Predicting tree mortality is especially challenging given the multiple pathways through which climate can induce mortality and the ways in which different species respond to climate change. Specifically, mortality due to water limitation can result from long-term shifts in climate, specific extreme events or their interaction[2,4,13,14]. For example, temperature could increase tree mortality directly by increasing physiological thermal stress[15,16] or indirectly by increasing atmospheric evaporative demand (that is, vapour pressure deficit (VPD))[7,17–20], whereas increasing seasonality in the tropics and subtropics would increase soil water stress and decrease dry season water supply[21]. These processes increase the probability of death through a series of potential mechanisms (for example, hydraulic failure or carbon starvation[7,13,14,22,23]). In particular, some studies suggest that tropical forests on the drier edge of the biome’s range may be closer to a tolerance threshold and hence more vulnerable to water stress, as revealed by reductions in growth[24], increases in mortality[25,26] and decreases in population size[27,28]. However, other work suggests that compositional diversity in forests near this dry edge might provide buffers against forest dieback, with some taxa or regions suffering less from water stress[3,6]. Improving our understanding of mortality dynamics requires quantifying mortality patterns along climatic

---

[1]Smithsonian Environmental Research Center, Edgewater, MD, USA. [2]Environmental Change Institute, School of Geography and the Environment, University of Oxford, Oxford, UK. [3]AMAP (Botanique et Modélisation de l’Architecture des Plantes et des Végétations), Université de Montpellier, CIRAD, CNRS, INRAE, IRD, Montpellier, France. [4]Ecosystem Stewardship, Royal Botanic Gardens Kew, London, UK. [5]Centre for Tropical Environmental and Sustainability Science, College of Science and Engineering, James Cook University, Cairns, Queensland, Australia. [6]Department of Biology, Sonoma State University, Rohnert Park, CA, USA. [7]ARC Centre of Excellence for Climate Extremes, University of New South Wales, Sydney, New South Wales, Australia. [8]Department of Environmental Science, Policy, and Management, UC Berkeley, Berkeley, CA, USA. [9]Biodiversity Dynamics, Naturalis Biodiversity Center, Leiden, The Netherlands. [10]School of Geography, University of Leeds, Leeds, UK. [11]Southwest Biological Science Center, U.S. Geological Survey, Moab, UT, USA. [12]CSIRO Land and Water, Tropical Forest Research Centre, Atherton, Queensland, Australia. [13]Fenner School of Environment and Society, The Australian National University, Canberra, Australian Capital Territory, Australia. [14]Universidad Nacional San Antonio Abad del Cusco, Cusco, Perú. ✉e-mail: david.bauman@oxfordecosystems.co.uk

gradients with an explicit consideration of taxon-level vulnerability to environmental constraints. As such, long-term demographic datasets along these gradients are uniquely capable of disentangling patterns in mortality from their potential mechanisms in a way that can inform predictions[29]. However, analyses of the infrequent and stochastic nature of mortality require sustained, long-term monitoring, which is rare, especially in the tropics.

Using tropical forest demographic data spanning 49 years, we analysed temporal patterns of tree mortality for 81 dominant tree species encompassing 74,135 observations of stems above 10 cm in diameter across 24 tropical moist forest plots along an elevation gradient in North Queensland, Australia (Supplementary Tables 1, 2). We estimated the probability of mortality (hereafter 'mortality risk') across stems, species, plots and years (eq. 1 in Methods; Extended Data Figs. 1, 2). Analysing the yearly distribution of mortality risk across all plots and species from 1971 through 2019 (model M1; see Methods), we show that after a period of slight mortality risk decline, the baseline risk increased, with several years standing out as high-risk years. A change-point analysis on these data confirmed a transition from moderately decreasing to increasing mortality risk occurring in the mid-1980s (the analysis indicating 1984) (model M2; Supplementary Tables 3, 4). This modelled shift is also evident in the observed mortality rates across plots and census intervals (Fig. 1b). The mechanisms responsible for the increase in mortality risk are associated with secular long-term climate change (notably an increase in temperature and atmospheric water VPD) (Fig. 1c) and wind-disturbance events due to cyclones (black triangles in Fig. 1b).

The mortality risk estimated per stem and year from the census data were used as response variables in a series of Bayesian multilevel analyses (models M1–M6; Supplementary Table 4) to test temporal patterns of mortality risk after 1984 across plots and species and to investigate potential underlying mechanisms associated with those patterns. We focused on the effect of VPD and maximum daily air temperature (*T*max) to explain differences in both average mortality risk and its rates of change over time among plots, as both VPD and temperature have increased in all 24 plots in the past 49 years and have reduced tree growth[24] (Fig. 1c), and are candidates in increasing forest stress globally[2,30,31]. To capture the potential influence of soil water supply on tree water stress and rainfall seasonality, we also used maximum climatological water deficit (MCWD) as an additional predictor. Specifically, we used *T*max and VPD of the driest quarter of the year, and MCWD, averaged over 35 years (1984–2019; M3; see Supplementary Table 4).

We found an increase in plot-level average mortality risk between 1984 and 2019 in 21 of the 22 plots with at least three censuses (Figs. 2, 3a, Supplementary Table 5; grand 'year' slope (eq. 3): $\beta_0 = 0.23$ (0.29–0.17), median and 95% highest posterior density interval (HPDI)) with a five-fold difference in the rate of mortality risk change over time along the climate gradient ('among-plot' variation in the year slope: $\sigma_\beta = 0.16$ (0.12–0.21); Fig. 3a; see eq. 3 in Supplementary Methods 1). Model predictions indicated a doubling in average mortality risk across plots between the 1980s and 2010s (model M3; Fig. 3a), corresponding to a potential halving of tree life expectancy and carbon residence time[32]. None of the mean climate predictors explained the variation in the slope of temporal change of mortality risk among plots (Extended Data Fig. 3, Supplementary Table 5); drier plots were no more vulnerable to increased mortality risk than more moist plots. However, the overall plot-specific average mortality risk (α_k; eq. 3) was higher in warmer and drier plots (Fig. 2, Extended Data Fig. 3; α_1 (VPD): 0.30 (0.49–0.12) and α_1 (*T*max): 0.37 (0.52–0.23)). Plot average MCWD showed no evidence of an association with mortality risk (Supplementary Table 5). Cyclones occurred in a subset of plots (triangles in Fig. 1b), so we tested whether the increase in mortality risk could be due to cyclone occurrence alone. We performed two reanalyses of the full model construction using (1) all plots, but with any census interval with observed cyclone occurrence removed, and (2) only plots with no cyclone disturbances in the past 50 years. In both cases, there remained a marked increase in mortality risk across years following 1984 (Extended Data Fig. 4, Supplementary Table 6), suggesting that another mortality cause was driving, and possibly interacting with, wind disturbance events, to increase mortality risk across the plots.

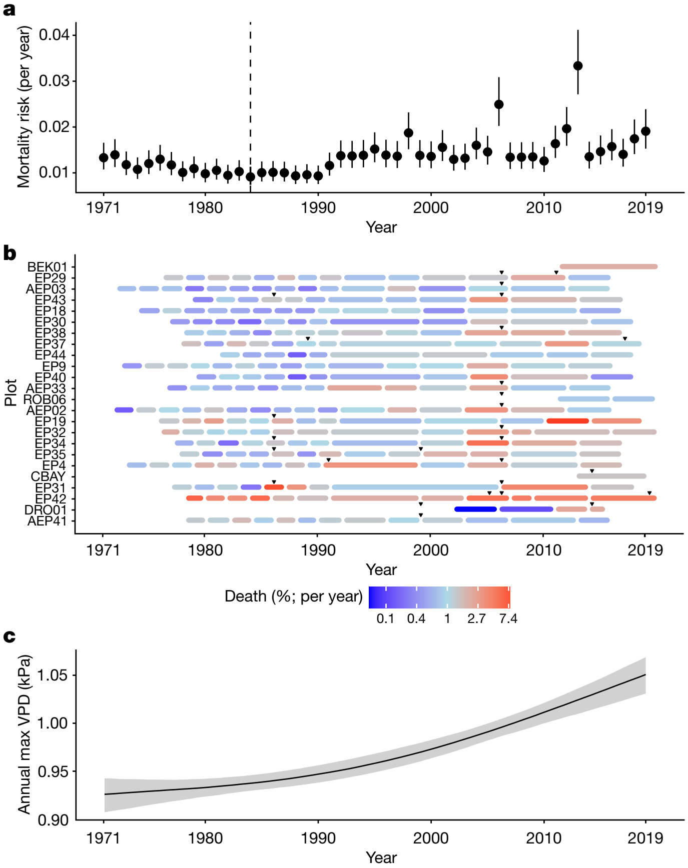

Fig. 1 | Temporal increase of modelled annual mortality risk, annualized observed percentage of tree death and atmospheric VPD across the 24 studied plots. a, Temporal variation of the modelled latent mortality risk per year across all 24 plots and 81 species, with a change point identified in 1984 (dashed line) that marks the beginning of an increase (see Supplementary Table 3). The circles and intervals are median and 95% highest posterior density intervals (HPDIs), respectively, of the year-specific mortality risk (see M2, Supplementary Table 4). **b**, Annualized percentage of tree death per plot and census interval, indicating a temporal increase across all plots, partly but not only related to wind damage from cyclones (black triangles). **c**, Predicted temporal increase of maximum annual VPD across all 24 plots. The line and shaded area are median and 95% HPDIs, respectively, for VPD predicted from the model fit (see Methods).

To evaluate whether some taxa were particularly vulnerable to changing climate, we tested how the mortality risks of species changed after 1984 (model M4), and examined how their local distributions related to their total geographical range (model M5), and whether some traits correlated with their average mortality risk or rate of mortality risk increase (model M6). Model M4 confirmed a general increase in mortality risk over time across species ($\beta_0 = 0.17$ (0.21–0.14); Fig. 4a, b, Supplementary Table 4), with 70% of the species presenting the trend (Fig. 3b) and substantial variability across species (σ_β: 0.19 (0.16–0.21); see eq. 4) (Fig. 3b). The average annual mortality risk for species varied between 0.007 and 0.051 (mean of 0.021; Supplementary Table 2).

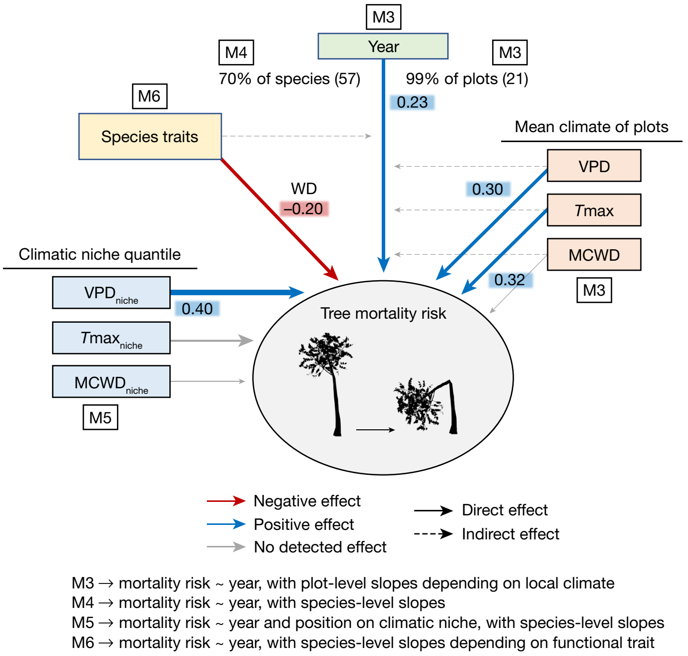

Fig. 2 | Temporal increase of tree mortality risk and influence of the mean climate of plots, the position of species on their climatic niche and functional traits on mortality risk. Results displayed from the Bayesian multilevel models M3 to M6 investigating different aspects of the mortality risk pattern (Supplementary Table 4). The red and blue arrows represent clear negative and positive effects on mortality risk, respectively, whereas the grey arrows indicate that no clear effect was detected (that is, slope coefficients whose 95% - HPDIs encompassed zero). The solid and dashed arrows illustrate direct and indirect effects on tree mortality risk, respectively, in which indirect effects affect mortality risk by accentuating or attenuating the direct effect of 'year' (details in Supplementary Methods 1). Coefficients from different models cannot be directly compared, as they arise from models using different subsets of the dataset (see Methods; Supplementary Table 4). The palm vector was created by kjpargeter (www.freepik.com). WD, wood density. The tilde symbols (~) denote 'modelled as a function of'; see Supplementary Methods 1 for details of models M3 to M6 in Supplementary Methods 1).

Although the increasing mortality trend across species and plots in our analysis is clear, attributing this trend to specific causes is challenging. Mortality can lag its cause by months to years[33–37] and any single mortality event can be due to multiple interacting causes[34,36,38–40]. Available meteorological data cannot perfectly capture the mortality mechanisms due to spatial and temporal precision, or accurate representation of the driving mechanism (that is, the disconnect between high VPD, embolism, vascular failure and crown death). Finally, observations of mortality in censuses do not represent the exact year of death. We attempted to extend our inference from the observed mortality risk pattern to possible attribution in three ways: (1) linking geographical ranges to plot-level patterns among species, (2) testing trait relationships to the mortality shift, and (3) investigating cyclone occurrence and the plot-specific and species-specific mortality risk trends.

Many of the species in our plots are widespread across tropical Southeast Asia, offering a robust assessment of climate niche. Climate niches were approximated for 56 of the 81 species that occurred in at least four of the 24 plots, using a projection of presences across climate space built by combining all recorded species occurrences with a 30-year climatology of maximum VPD, temperature and MCWD. We then expressed each of our plot mean climate metrics in terms of quantiles on the total univariate climatic niche of each species, yielding variables of species position on their broader geographical climate niche ($\mathrm{VPD_{niche}}$, $T\mathrm{max_{niche}}$ and $\mathrm{MCWD_{niche}}$; Fig. 4). Model M5 regressed mortality risk after 1984 on these three niche-related covariates, with year to control for the temporal increase and with species-level slopes for all covariates (see eq. 5). The average mortality risk was higher the closer species were to the drier edge of their range (that is, the upper limit of their VPD niche; $\beta_{3,0}$: 0.40 (0.27–0.52); Figs. 2, 4, Supplementary Table 5). This increase in average mortality risk with $\mathrm{VPD_{niche}}$ affected 79% of the 56 species (Fig. 4). A similar, although less-marked, increase in average mortality risk occurred closer to the upper edge of the $T\mathrm{max_{niche}}$ when considering a 90% HPDI ($\beta_{2,0}$: 0.13 (0.01–0.24); eq. 5). This $T\mathrm{max_{niche}}$ effect increased when removing $\mathrm{VPD_{niche}}$ from the model, indicating that $T\mathrm{max_{niche}}$ is associated with mortality risk indirectly through $\mathrm{VPD_{niche}}$ (see sensitivity analysis in Supplementary Methods 1, Supplementary Table 5). The position on the MCWD niche had no clear effect across species (Supplementary Table 4).

Functional traits may indicate distinct mortality vulnerabilities among species. Forty of the studied species had functional trait measurements, including morpho-anatomical features such as leaf mass per area and wood density, chemical traits such as leaf C stable isotope ratio, leaf nitrogen and phosphorus, and gas exchange traits such as stomatal conductance and maximum photosynthetic capacity (Extended Data Fig. 5, Supplementary Table 7). To test for physiological mechanisms that potentially underlie interspecific differences in the pace of mortality risk change over time, we used the subset of 40 species with trait data in a modified version of M4 to see whether the mean trait values of species predicted an average risk for species and the temporal change in that risk post-1984 (model M6; Supplementary Table 4). Wood density (a proxy for mechanical strength and embolism resistance[41,42]) showed a clear negative relationship with average mortality risk (α_1: −0.21 (−0.38 to −0.05); eq. 6). However, no traits predicted the variation among species in the temporal change (that is, the slope) of the mortality risk (Fig. 2, Extended Data Fig. 6). This lack of a signal could be due to using species average traits or limited sample sizes in focusing on species across plots as well as the potential for a null or minor effect[34,43].

Wind damage contributes to tree mortality and carbon cycling in other tropical forests[44–46] and the prevalence of cyclone impacts recorded in a number of plots here indicate that wind may have contributed to the increase in mortality risk directly or indirectly. Whereas wind-related events often determine the moment of tree death, other abiotic and biotic risk factors are key in determining tree vulnerability to storms, highlighting the importance of interactions among multiple risk factors in determining tree death[22,34,36,40]. In particular, VPD is likely to increase tree vulnerability to wind damage, as well as to other risk factors such as biotic agents[34,36], in addition to its direct water-related stress[17,47].

Mortality changes in tropical forests have been associated with climate events such as droughts, which will impact long-term forest dynamics if they become more pervasive[1,48,49]. Here, MCWD did not explain average mortality risk across plots nor showed any clear temporal trend associated with mortality risk (Extended Data Fig. 11; Bauman et al.[24]). Further exploring how chronically increasing VPD (presses[50]) interacts with heat waves, drought events and more frequent extreme VPD anomalies (pulses[50]) to affect long-term mortality trends will be important to better quantify a causal link between climate change and tree mortality. Our study indicates, whether due to particular events or accumulated vulnerability, a consistent increase in mortality. When compounded over large areas for long periods of time, this mortality increase can result in changes in forest dynamics, structure, composition and carbon residence time[32,51]. Increasing a typical tree mortality rate from 1% to 2% per year, for instance, halves tree life expectancy, carbon residence time and, in the absence of increases in forest-wide productivity, long-term biomass stocks[32].

To test potential effects of the mortality increase on stand structure, we tested whether decreases in plot-level basal area (used as a proxy for above-ground biomass) were offset by subsequent increases in basal

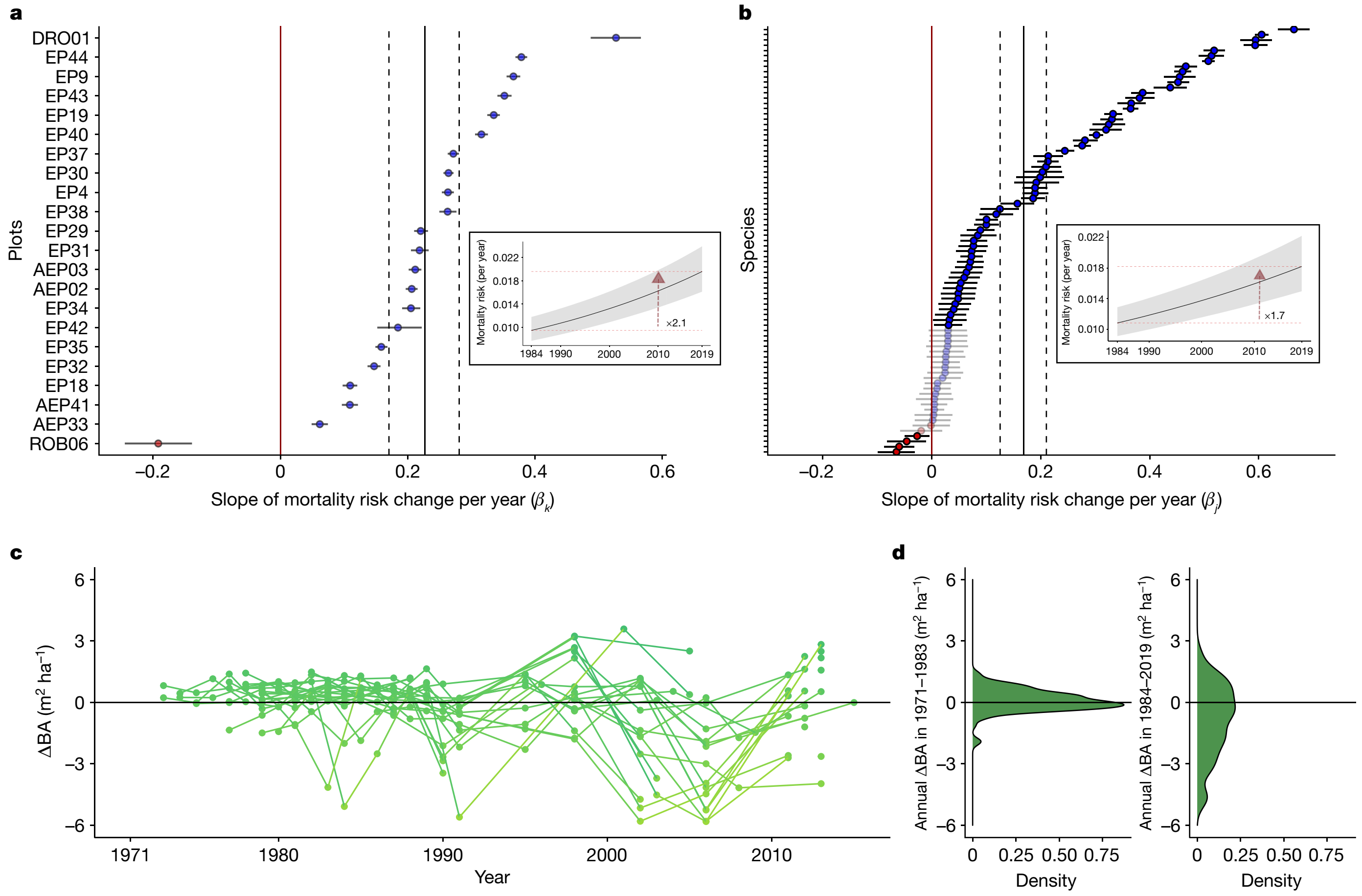

Fig. 3 | Plot-level and species-level temporal changes of annual mortality risk (1984–2019) and change of plot basal area between consecutive censuses. a, **b**, Circles and intervals are median and 95% - HPDIs, respectively, of plot-level (**a**) and species-level (**b**) 'year' slope coefficient posteriors (β_k and β_j, respectively; see eqs. 3 and 4), from models M3 and M4, respectively. Plots and species whose 95% - HPDI encompassed zero are half-transparent. The blue and red circles indicate clear temporal increases and decreases in mortality risk, respectively, at a 95% level of confidence (HPDI). The black vertical solid and dashed lines are the median and 95% - HPDI of the grand 'year' slope (that is, 'year' effect across plots (**a**) and species (**b**); β_0 in eqs. 3 and 4). The vertical red line highlights 0, beyond which mortality risk increased over time. Insets: model prediction of mortality risk per year for the period 1984–2019, showing the median (line) and 95% HPDI (shaded area) of the posterior distributions for the grand effect. model posterior predictions show approximately a doubling of mortality risk between 1984 and 2019 (2.1-fold and 1.7-fold increases at the plot and species levels, respectively). **a** and **b** show that mortality risk markedly increased across plots and species. **c**, Variation of ΔBA per plot over time, in which ΔBA is the change of basal area between consecutive censuses in a given plot ($\Delta BA_t = BA_t - BA t_{-1}$), such that positive values indicate an increase in BA from census $t-1$ to census t, and negative values indicate a decrease. Each circle is the ΔBA of a plot at the beginning of a census period, and lines connect consecutive observations for each plot. The colour of line segments, between two circles, is proportional to the corresponding ΔBA. **d**, Density distribution of the annualized ΔBA based on consecutive plot censuses, before and after the change point of 1984. **c** and **d** show that BA losses due to mortality were not offset by BA gains related to growth and recruitment into the census.

area due to growth and recruitment into the census. We found a clear decline in basal area over the monitoring period, in line with a previous study[52] (Fig. 3c, d, Extended Data Fig. 7). The change in basal area between censuses (that is, drops or gains) showed an increasing number and extent of drops (Fig. 3c), and these were not offset by gains (Fig. 3c, d). Over the period studied, plots lost approximately 230.2 m^2 ha^{-1} but gained only 113.7 m^2 ha^{-1}, a 12.2% decline from the basal area of the first census of each plot, converting these forests into biomass carbon sources. Although some studies have suggested that large trees are more vulnerable to water stress due to height-driven hydraulic vulnerability, which could have disproportionate consequences for biomass change[14,53], we found no evidence of this here (Extended Data Fig. 8), in line with recent works[34].

Our study shows that (1) mortality risk increased across plots and species, (2) tropical cyclones alone cannot explain the pattern, (3) average mortality risk is higher in drier plots and at the drier edge of the geographical range of most species, (4) VPD displays a temporal increase in all plots that corresponds to the mortality risk increase (unlike MCWD), and is a known physiological stressor and mortality risk factor[8,17], and (5) there is no evidence that the increase in mortality risk is driven by increases in growth rates (see Extended Data Fig. 9, Supplementary Methods 1). Tree growth was also recently shown to be reduced by positive VPD anomalies in the region, with fast-growing species as well as drier plots being more suppressed[24]. Although acknowledging the contribution of wind disturbances and other unaccounted for mortality risk factors such as lightning, the above elements provide evidence that a chronic long-term increase in atmospheric evaporative demand may increase mortality risk in moist tropical forests of Australia. This is supported by similar findings in the Amazon and African tropical forests[1,2] and when comparing key climate variables across our plots to the climate of moist tropical forest globally: VPD, *T*max, annual precipitation and climatic water deficit at our plots encompassed 31%, 23%, 74% and 40% of global-scale tropical moist forest climatic space, respectively (Extended Data Fig. 10). The near-ubiquitous nature of temperature and VPD rise across the tropics suggests that this phenomenon may be responsible for, and may

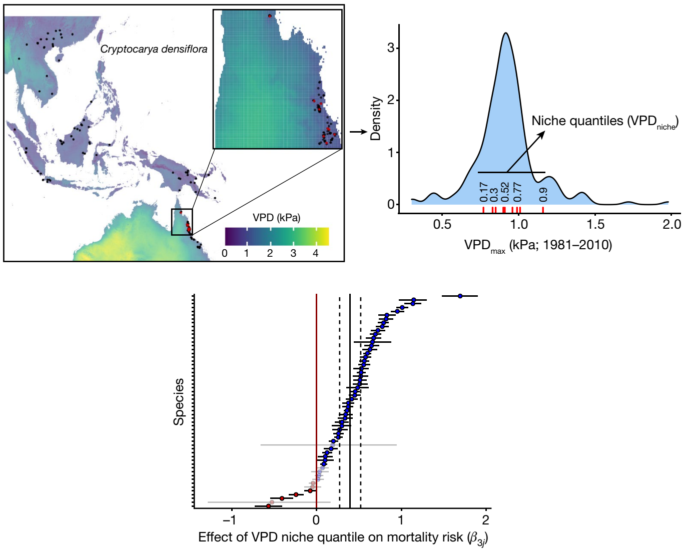

Fig. 4 | Spatial effect of the proximity of species from the upper limit of their VPD niche on the average mortality risk (model M5). The upper part of the figure illustrates for one species (*Cryptocarya densiflora Blume*) the calculation of the VPD niche quantiles (VPD$_{niche}$) for species in the study plots where the species occur (red circles), on the basis of its total biogeographical distribution (sum of black and red circles), its climatic niche calculated based on a 30-year climatology (map background) of the locations where the species was observed (density plot), and the mean VPD$_{max}$ in the studied plots where the species is (red bars at the bottom of the density plot). The lower part of the figure shows the effect of VPD$_{niche}$ on the average mortality risk per species (β_{3j}) and across species ($\beta_{3,0}$; vertical solid and dashed lines; see legend of Fig. 3 for circles, bars, and transparency, and eq. 5 in Supplementary Methods 1 for model details). Species at the upper end of their VPD niche are more likely to experience increased mortality risk; 79% of species have higher average mortality risk closer to the upper edge of their VPD niche.

in the future drive, an acceleration of tree mortality and concomitant decrease of living biomass across the tropics.

One potential buffer to the effects of climate change on diverse forests could be the various ways different species tolerate shifts in the conditions that lead to water[54,55] or temperature stress[56]. These strategies may be represented by the functional traits of species[14,42,55]. Higher wood density correlated with reduced average annual mortality risk, indicating potential roles for enhanced wood strength or resistance to embolism[41,42]. Here, none of the measured traits explained the interspecific variation in the temporal increase in mortality risk. However, we cannot rule out that other traits (for example, hydraulic safety margin and xylem vulnerability to embolism[5,34,55]) might better explain changes in mortality risk across species. Australian moist tropical forest species, in particular, have been shown to have narrower hydraulic safety margin than species growing in drier forests[42].

Some of the challenges in attributing mechanisms to mortality observations are unavoidable, such as the lag between cause and consequence of death, but intensified monitoring protocols and new technologies should improve attribution[36,39,57]. In addition to long-term plot monitoring, mortality attribution can be improved with focused collections of environmental stressors at high frequency (for example, micrometeorology and soil moisture at depth), as well as higher-frequency monitoring of individual tree death (for example, annual or even seasonal mortality surveys[36,39,57]). Better assessment of tree health through methods as focused as sap flux or as broad as remote sensing of leaf function could also improve our ability to assign cause to individual mortality events. Such intensified monitoring programmes should improve representation of mortality risk in vegetation models, a crucial advance to better predict the future pathway of the tropical forest carbon sink, and hence the remaining anthropogenic carbon budget available to stay well below 2 °C peak global warming.

Online content

Any methods, additional references, Nature Research reporting summaries, source data, extended data, supplementary information, acknowledgements, peer review information; details of author contributions and competing interests; and statements of data and code availability are available at https://doi.org/10.1038/s41586-022-04737-7.

1. Brienen, R. J. W. et al. Long-term decline of the Amazon carbon sink. *Nature* **519**, 344–348 (2015).
2. Hubau, W. et al. Asynchronous carbon sink saturation in African and Amazonian tropical forests. *Nature* **579**, 80–87 (2020).
3. Zuleta, D., Duque, A., Cardenas, D., Muller-Landau, H. C. & Davies, S. J. Drought-induced mortality patterns and rapid biomass recovery in a terra firme forest in the Colombian Amazon. *Ecology* **98**, 2538–2546 (2017).
4. Phillips, O. L. et al. Drought sensitivity of the Amazon rainforest. *Science* **323**, 1344–1347 (2009).
5. Powers, J. S. et al. A catastrophic tropical drought kills hydraulically vulnerable tree species. *Glob. Chang. Biol.* **26**, 3122–3133 (2020).
6. Bennett, A. C. et al. Resistance of African tropical forests to an extreme climate anomaly. *Proc. Natl Acad. Sci. USA* **118**, e2003169118 (2021).
7. Brodribb, T. J., Powers, J., Cochard, H. & Choat, B. Hanging by a thread? Forests and drought. *Science* **368**, 261–266 (2020).
8. McDowell, N. G. *et al.* Pervasive shifts in forest dynamics in a changing world. Science 368, (2020).
9. Pan, Y. et al. A large and persistent carbon sink in the world's forests. *Science* **333**, 988–993 (2011).
10. Matthews, H. D. et al. An integrated approach to quantifying uncertainties in the remaining carbon budget. *Commun. Earth Environ.* **2**, 7 (2021).
11. Girardin, C. A. J. et al. Nature-based solutions can help cool the planet—if we act now. *Nature* **593**, 191–194 (2021).
12. Friedlingstein, P. et al. *Earth Syst. Sci. Data* 14, 1917–2005 (2022)
13. Choat, B. et al. Triggers of tree mortality under drought. *Nature* **558**, 531–539 (2018).
14. Rowland, L. et al. Death from drought in tropical forests is triggered by hydraulics not carbon starvation. *Nature* **528**, 119–122 (2015).
15. Lloyd, J. & Farquhar, G. D. Effects of rising temperatures and [CO$_2$] on the physiology of tropical forest trees. *Phil. Trans. R. Soc. B* **363**, 1811–1817 (2008).
16. O'Sullivan, O. S. et al. Thermal limits of leaf metabolism across biomes. *Glob. Chang. Biol.* **23**, 209–223 (2017).
17. Grossiord, C. et al. Plant responses to rising vapor pressure deficit. *New Phytol.* **226**, 1550–1566 (2020).
18. Rifai, S. W., Li, S. & Malhi, Y. Coupling of El Niño events and long-term warming leads to pervasive climate extremes in the terrestrial tropics. *Environ. Res. Lett.* **14**, 105002 (2019).
19. Rifai, S. W. et al. ENSO drives interannual variation of forest woody growth across the tropics. *Phil. Trans. R. Soc. B* **373**, 20170410 (2018).
20. Smith, M. N. et al. Empirical evidence for resilience of tropical forest photosynthesis in a warmer world. *Nat. Plants* **6**, 1225–1230 (2020).
21. Malhi, Y. et al. Exploring the likelihood and mechanism of a climate-change-induced dieback of the Amazon rainforest. *Proc. Natl Acad. Sci. USA* **106**, 20610–20615 (2009).
22. McDowell, N., Allen, C. D. & Anderson-Teixeira, K. Drivers and mechanisms of tree mortality in moist tropical forests. *New Phytol.* **219**, 851–869 (2018).
23. McDowell, N. et al. Mechanisms of plant survival and mortality during drought: why do some plants survive while others succumb to drought? *New Phytol.* **178**, 719–739 (2008).
24. Bauman, D. et al. Tropical tree growth sensitivity to climate is driven by species intrinsic growth rate and leaf traits. *Glob. Chang. Biol.* **28**, 1414–1432 (2022).
25. Esquivel-Muelbert, A. et al. Tree mode of death and mortality risk factors across Amazon forests. *Nat. Commun.* **11**, 5515 (2020).
26. Anderegg, W. R. L., Anderegg, L. D. L., Kerr, K. L. & Trugman, A. T. Widespread drought-induced tree mortality at dry range edges indicates that climate stress exceeds species' compensating mechanisms. *Glob. Chang. Biol.* **25**, 3793–3802 (2019).
27. Aguirre-Gutiérrez, J. et al. Drier tropical forests are susceptible to functional changes in response to a long-term drought. *Ecol. Lett.* **22**, 855–865 (2019).
28. Aguirre-Gutiérrez, J. et al. Long-term droughts may drive drier tropical forests towards increased functional, taxonomic and phylogenetic homogeneity. *Nat. Comm.* **11**, 3346 (2020).
29. Meir, P., Mencuccini, M. & Dewar, R. C. Drought-related tree mortality: addressing the gaps in understanding and prediction. *New Phytol.* **207**, 28–33 (2015).
30. Sullivan, M. J. P. et al. Long-term thermal sensitivity of Earth's tropical forests. *Science* **368**, 869–874 (2020).
31. Yuan, W. et al. Increased atmospheric vapor pressure deficit reduces global vegetation growth. *Sci. Adv.* **5**, eaax1396 (2019).
32. McMahon, S. M., Arellano, G. & Davies, S. J. The importance and challenges of detecting changes in forest mortality rates. *Ecosphere* **10**, e02615 (2019).
33. Trugman, A. T. et al. Tree carbon allocation explains forest drought-kill and recovery patterns. *Ecol. Lett.* **21**, 1552–1560 (2018).

34. Trugman, A. T., Anderegg, L. D. L., Anderegg, W. R. L., Das, A. J. & Stephenson, N. L. Why is tree drought mortality so hard to predict? *Trends Ecol. Evol.* **36**, 520–532 (2021).
35. Phillips, O. L. et al. Drought–mortality relationships for tropical forests. *New Phytol.* **187**, 631–646 (2010).
36. Aleixo, I. et al. Amazonian rainforest tree mortality driven by climate and functional traits. *Nat. Clim. Change* **9**, 384–388 (2019).
37. Lingenfelder, M. & Newbery, D. M. On the detection of dynamic responses in a drought-perturbed tropical rainforest in Borneo. *Plant Ecol.* **201**, 267–290 (2009).
38. McDowell, N. G. et al. The interdependence of mechanisms underlying climate-driven vegetation mortality. *Trends Ecol. Evol.* **26**, 523–532 (2011).
39. Zuleta, D. et al. Individual tree damage dominates mortality risk factors across six tropical forests. *New Phytol.* **233**, 705–721 (2022).
40. Fontes, C. G. *et al*. Dry and hot: the hydraulic consequences of a climate change-type drought for Amazonian trees. Phil. Trans. R. Soc. B 373, 20180209 (2018).
41. Chave, J. et al. Towards a worldwide wood economics spectrum. *Ecol. Lett.* **12**, 351–366 (2009).
42. Peters, J. M. R. et al. Living on the edge: a continental-scale assessment of forest vulnerability to drought. *Glob. Chang. Biol.* **27**, 3620–3641 (2021).
43. Yang, J., Cao, M. & Swenson, N. G. Why functional traits do not predict tree demographic rates. *Trends Ecol. Evol.* **33**, 326–336 (2018).
44. Espírito-Santo, F. D. B. et al. Size and frequency of natural forest disturbances and the Amazon forest carbon balance. *Nat. Commun.* **5**, 3434 (2014).
45. Chambers, J. Q. et al. The steady-state mosaic of disturbance and succession across an old-growth Central Amazon forest landscape. *Proc. Natl Acad. Sci. USA* **110**, 3949–3954 (2013).
46. Rifai, S. W. et al. Landscape-scale consequences of differential tree mortality from catastrophic wind disturbance in the Amazon. *Ecol. Appl.* **26**, 2225–2237 (2016).
47. López, J., Way, D. A. & Sadok, W. Systemic effects of rising atmospheric vapor pressure deficit on plant physiology and productivity. *Glob. Chang. Biol.* **27**, 1704–1720 (2021).
48. Brando, P. M. et al. Abrupt increases in Amazonian tree mortality due to drought\ textendashfire interactions. *Proc. Natl Acad. Sci. USA* **111**, 6347–6352 (2014).
49. Phillips, O. L. et al. Pattern and process in Amazon tree turnover, 1976–2001. *Phil. Trans. R. Soc. Lond. B* **359**, 381–407 (2004).
50. Harris, R. M. B. et al. Biological responses to the press and pulse of climate trends and extreme events. *Nat. Clim. Change* **8**, 579–587 (2018).
51. Andrus, R. A., Chai, R. K., Harvey, B. J., Rodman, K. C. & Veblen, T. T. Increasing rates of subalpine tree mortality linked to warmer and drier summers. *J. Ecol.* **109**, 2203–2218 (2021).
52. Murphy, H. T., Bradford, M. G., Dalongeville, A., Ford, A. J. & Metcalfe, D. J. No evidence for long-term increases in biomass and stem density in the tropical rain forests of Australia. *J. Ecol.* **101**, 1589–1597 (2013).
53. Bennett, A. C., McDowell, N. G., Allen, C. D. & Anderson-Teixeira, K. J. Larger trees suffer most during drought in forests worldwide. *Nat. Plants* **1**, 15139 (2015).
54. Chitra-Tarak, R. et al. Hydraulically-vulnerable trees survive on deep-water access during droughts in a tropical forest. *New Phytol.* **231**, 1798–1813 (2021).
55. Anderegg, W. R. L. et al. Meta-analysis reveals that hydraulic traits explain cross-species patterns of drought-induced tree mortality across the globe. *Proc. Natl Acad. Sci. USA* **113**, 5024–5029 (2016).
56. Taylor, T. C., Smith, M. N., Slot, M. & Feeley, K. J. The capacity to emit isoprene differentiates the photosynthetic temperature responses of tropical plant species. *Plant Cell Environ.* **42**, 2448–2457 (2019).
57. Arellano, G., Zuleta, D. & Davies, S. J. Tree death and damage: a standardized protocol for frequent surveys in tropical forests. *J. Veg. Sci.* **32**, e12981 (2021).

Methods

Site and species data

The dataset encompasses 49 years of inventory data from 24 tropical moist forest plots distributed along an elevation gradient ranging between 15 and 1,500 m above sea level, and censused on average 12 times, in northern Queensland, Australia, between −12.73 to −21.25 and 143.25 to 148.55 (see details in Supplementary Table 1 and ref. [24]). Each census consisted of the measurement of all trees above 10 cm diameter at breast height (DBH). Twenty plots (0.5 ha, 100 × 50 m) were established between 1971 and 1980 to provide long-term ecological and demographic data[58], whereas four plots were established more recently along the same elevation gradient (Supplementary Table 1). With two exceptions, the plots were established in unlogged forest; at establishment, EP9 and EP38 showed localised evidence of disturbance due to selective logging at least 20 years before[58]. Cyclonic disturbance contributes to the dynamics of the forests[52], with at least one plot affected by cyclones in 1986, 1989, 1999, 2006, 2011, 2014, 2017 and 2019 (Fig. 1b). The gradient covers a wide range of mean annual temperatures (19–26.1 °C), precipitation (1,213–3,563 mm) and mean VPD (6.5–11.8 hPa) (Supplementary Table 1). All trees with stems 10 cm or more DBH were mapped, identified to species level and measured for diameter. The 20 long-term plots were remeasured every 2 years for 10 years, and then at 3–4-year intervals, with diameter, recruits and deaths recorded, summing up to 11–17 censuses per plot. The remaining four plots were established more recently, between 2001 and 2012, and were resampled one to three times (Supplementary Table 1).

The initial dataset comprised 110,551 observations, from 13,513 individual stems from 535 species, in 54 genera and 79 families (details in Supplementary Table 2 of Bauman et al.[24]). We used a cut-off of a minimum of 400 observations per species to model the functional size dependence of survival of a species (see ‘Estimating tree survival across size, space and time’ section), to ensure sufficient statistical power (species list and sampling features in Supplementary Table 2). This resulted in a dataset of 81 tree species, 8,314 individual stems, 74,135 observations and 492 death events over the 49 years across the 24 forest plots. Species were found in between 1 and 16 plots, with a mean of 6.1, and individual stems were censused 2–17 times (mean 10.4) over periods of 2–44 years (mean 13 years) (Supplementary Table 2).

Estimating tree survival across size, space and time

The basis of all downstream analyses was the estimation of the yearly probability of survival (a latent, or unobserved, variable) from fitting a survival function to each species separately in a multilevel model framework, with ‘plot’ and ‘year’ as varying effects (also often referred to as ‘random effects’). The first step of our approach consisted of estimating size-dependent tree survival by fitting a functional form to every species separately, across the multiple censuses and forest plots where it occurred. The model we developed to characterize tree survival was built on the work of recent studies[59,60], combining the same five survival parameters into an S-shaped and inverse S-shaped logistic function of survival probability (Extended Data Fig. 1; eqs. 1.4, 1.5; see model details in Supplementary Methods 1). These correspond to the baseline survival probability per year (*K*; survival probability for most of the adult life of an individual), the rate of survival increase until reaching the arbitrary size where the survival probability becomes *K* (*r*1), the size corresponding to the inflexion point of the first S-shaped portion of the functional form (*p*1), and the corresponding *r*2 and *p*2 parameters for the inverse S-shaped portion of the functional form, corresponding to the yearly rate of survival decrease when the species approaches its maximum size, and the inflexion point corresponding to the size at which the yearly survival probability is 50% (species stature), respectively (Extended Data Fig. 1; illustration for four species in Extended Data Fig. 2).

In this study, we sought to investigate temporal changes in the survival probability per year (*K*) over the past 50 years, whether they vary across space (forest plots along a climatic gradient) and species, and test whether long-term climate, the biogeographical range of species and species traits mediate these temporal patterns.

For each species separately, we modelled the logit-scaled *K* as a function of a species-specific mean *K* (*K*_*μ*) from which deviations arise from different plots (*K*_*P*) and years (*K*_*T*) (Extended Data Fig. 1; eq. 1.2). Instead of modelling the survival rate over the actual census period (mostly between 2 and 5 years; see ref. [24]), we took advantage of having different plots whose starting and ending census years differed and partly overlapped (Fig. 1b) to generate a latent variable of logit-scaled probability of survival *K* per plot and year (hereafter *K*_lat; Fig. 1; eq. 1.2). The real observations of binary survival outcomes (eq. 1.1) per stem per census *t* were thus used to generate latent probabilities of survival for every year encompassed by the period between consecutive censuses. Our Bayesian framework allowed estimating a posterior distribution of *K*_lat for each latent observation (that is, stem per plot per year; Extended Data Fig. 9), as:

$$\text{Survival}_{i,k,t} \sim \text{Bernoulli}(\theta) \quad (1.1)$$

$$\text{for}(x \text{ in } \quad \text{year\_0}_i \quad \text{year\_1}_i)\{$$

$$K\_\text{lat} = K\_\mu + K\_P_i + K\_T_{i,x} + \epsilon_i \quad (1.2)$$

$$K = \text{inv\_logit}(K\_\text{lat}) \quad (1.3)$$

$$\theta = \begin{cases} \dfrac{K}{1+\exp^{(-r1\times(\text{DBH}_i - p1))}}, \text{DBH}_i < \text{threshold} \quad (1.4) \\ \dfrac{K}{1+\exp^{(-r2\times(\text{DBH}_i - p2))}}, \text{DBH}_i \geq \text{threshold} \quad (1.5) \end{cases}$$

$$\}$$

$$K\_\mu \sim \text{Normal}(2, 1) \quad (1.6)$$

$$K\_P \sim \text{Normal}(0, \sigma_P) \quad (1.7)$$

$$K\_T \sim \text{Normal}(0, \sigma_T) \quad (1.8)$$

$$\epsilon \sim \text{Normal}(0, \sigma_\epsilon) \quad (1.9)$$

wheresurvival outcomes were modelled through either one of the logistic functions corresponding to the S-shaped or inverse S-shaped functions (eqs. 1.4 and 1.5, respectively), depending on whether the corresponding individual presented a DBH smaller or bigger than a threshold, here set as the mean DBH of the species (see Supplementary Methods 1 for prior specifications).

We extracted the median of the *K*_lat posterior distribution per latent observation (that is, the survival probability of a given stem on a given year). The resulting distribution of median *K*_lat values combined across all 81 species and 24 plots was used as the main response variable in the following models to investigate temporal patterns of survival.

We focus on the variation across groupings (species, plot and year) with *K*_lat as it best summarizes mortality of trees through most of their lives (Extended Data Figs. 7, 8). Although the other parameters that offer insights into early and late mortality are very powerful for certain questions, allowing that the data are available, we decided against focusing on differential mortality of small individuals due to the minimum size threshold of 10 cm DBH, a size above which most stems function similarly (that is, seedling and sapling drought vulnerability would fall well below this threshold). We do, however, acknowledge that non-emergent trees above 10 cm DBH may experience buffered variations in VPD and other variables related to their below canopy position, which we do not account for here.

All following analyses were performed on the latent logit-survivorship (*K*_lat), model results and coefficients are reported in terms of mortality probability (hereafter mortality risk), in which annual mortality risk is defined as 1 − survival probability, and the coefficient signs from the models presented below had their sign inverted (for example, a negative effect on survivorship becomes a positive effect on mortality risk). Note that as our approach focuses on linking mortality to ontogeny through size, it precludes accounting for census-interval length biases that emerge when longer intervals miss mortality events of individuals that grow into the census diameter and die before being recorded[61].

As these biases will tend to increase mortality estimates for shorter census interval lengths and become more pronounced for smaller size classes, our study has, if anything, underestimated mortality after the census interval increased in the early 1980s (see Fig. 1b).

Statistical analyses

Our statistical analyses followed from our initial hypotheses about tropical forest survival patterns, but also from our initial findings as related to those patterns. Therefore, our analysis proceeded through different models that relied on different subsets of the data depending on the questions asked. We began by investigating trends in mortality risk across plots and species and then focused on aspects that included species subsets occurring in multiple plots, plot communities independent of species, and biogeographical inference about the species across the plots. The six models used are summarized in Supplementary Table 4 and the next section (detailed model explanations and all equations are in Supplementary Methods 1). Because mortality events are rare and stochastic, requiring a lot of data for inference, and because the six models have different requirements (see below), we settled on maximizing inference from each model over reducing the dataset to the smallest common dataset allowing model comparison at the cost of statistical power. Different subsets of the data were therefore used for models M3 to M6 (see Supplementary Tables 2, 4).

Temporal trends in survival

We first generated an unconditional multilevel model of *K*_lat across all 81 species (model M1 in Supplementary Table 4), for a visual assessment of a temporal trend in the average survivorship per year (see eq. 2 for model details in Supplementary Methods 1). M1 used varying intercepts (also known as 'random' intercepts) to model mortality risk (*K*_lat; that is, overall intercept or grand mean) and species-level, plot-level and year-level deviations from the grand mean. Because an increasing trend in tree mortality risk was apparent in the 1980s (Fig. 1a), we tested for a changepoint year.

Changepoint

We used a changepoint analysis to statistically test whether our time series of latent logit-survival probabilities (*K*_lat) has shifted in mean value and, if so, to identify the most likely year when this change occurred[32,62] (model M2; Supplementary Table 4). A changepoint from slightly negative to clearly positive temporal trend in mortality risk was identified in 1984, across all plots and species (Fig. 1a). All further analyses focused on the structure and potential causes of the increase in tree mortality risk in the 1984–2019 35-year period.

Explaining the 'post-changepoint' survivorship decline

Causes of individual tree mortality are difficult to assess directly due to time lags between mortality and its cause, tree deaths being most often attributable to multiple mechanisms[34,40,63–65], and delays between the mortality event and its detection[36,66,67]. Because of this, direct causal relationships between tree mortality and specific weather events or average climatic conditions of a census interval are not possible. Instead, we use different datasets and approaches to best attribute known potential drivers of tree mortality with the patterns identified in the long-term data.

Plot-level changes and local mean climate

We built a Bayesian hierarchical model exploring the post-1984 mortality risk increase within and across plots to test the proportion of plots showing an increase in mortality risk through time, and to test whether average mortality risk and mortality risk changes over time depended on the local mean climate (model M3 in Supplementary Table 4; details in eq. 3, Supplementary Methods 1). To do so, we used plot mean climate, defined as a 35-year local average per climatic variable (1984–2019, to match the main period of interest). We specifically considered the effect of the 30-year average of the VPD of the year driest quarter and maximum temperature of the year warmest quarter (*T*max), as both VPD and temperature have markedly increased in all 24 plots during the past 49 years and are important drivers of tree growth in these plots[24]. In addition, we examined the effect of the MCWD, a metric that serves as a proxy for the annual accumulated water stress over the dry season estimated as the cumulative deficit between precipitation and evapotranspiration[21,68,69]. These variables can all have an effect on survival through water stress or heat-related impairment of biochemical reactions (which are not captured explicitly in this study). The VPD and temperature data were collected from ANUClimate v.2.0 between 1971 and 2019 (ref. [70]), and the MCWD was calculated using precipitation data from ANUClimate v.2.0 and evapotranspiration data from TerraClimate[71].

Species-level changes and biogeographical expectations

We used a similar Bayesian multilevel model specification as the previous one, without climate variables, to focus on species-specific mortality risk change trajectories and to test the proportion of species showing an increase in mortality risk over time (model M4; Supplementary Table 4).

We then used a space-for-time substitution to test whether the temporal increase in mortality risk could be driven by the marked temporal increase of temperature and VPD (see main text). Specifically, we tested whether species had lower average survival rates in plots closer to the drier edge of their geographical range (upper limit of their total VPD niche). Similarly, the MCWD was used to approximate the rainfall seasonality niche for species. This approach takes into account general ecophysiological constraints as well as the evolutionary history of each species, as captured through the biogeographical range of conditions where they occur[72,73]. For example, a difference of 2 °C in the mean temperature of two plots could be associated with a higher baseline mortality for one species for which the warmer plot falls close to the edge of its temperature niche, whereas baseline mortality would remain the same for a species for which both plots are near the niche centre for species. This biogeographical niche approach allowed us to investigate potential mechanisms underlying temporal trends[74], as well as providing potential ecophysiological mechanisms underlying the temporal and spatial pattern[73,75,76].

To generate approximate univariate climate niches for each species and define the relative location of the studied plots in these niches, we first extracted all known occurrences of 78 species (see the next section) from the Global Biodiversity Information Facility online database (Supplementary Table 8). Our goal was to balance the simplicity of a presence-only analysis while avoiding biases that might underestimate niche breadth. We therefore first filtered out multiple occurrences of a species to keep only one sample per radius of 1 km, to reduce the risk of oversampling[77] (a 3-km radius filter yielded very similar results; results not shown). The filtered spatial locations of the 78 species occurrences were matched to a 1/24° map of the 30-year climatology (average over 1981–2010) of the maximum annual VPD, the maximum daily air temperature (*T*max) and the MCWD, obtained from TerraClimate[71]. The univariate climate niches for species were defined separately for *T*max, VPD and MCWD as the distribution of 30-year mean values from the pixels corresponding to the biogeographic distribution for each species (including our plots) (see upper part of Fig. 4). The local 30-year average climate of our 24 plots were then expressed in terms of quantiles for each species separately, based on the species-specific climatic niches generated, yielding $T\mathrm{max}_{\mathrm{niche}}$, $\mathrm{VPD}_{\mathrm{niche}}$ and $\mathrm{MCWD}_{\mathrm{niche}}$, that is, the position of the species on their total niche for the corresponding variable. The resulting quantiles are species-specific expressions of how close the 30-year mean climate variables in our plots are from the upper limit of the total climatic niche for species. We tested the robustness of our quantile approach with respect to potential imperfect sampling in part of the biogeographical area by rerunning the M5 model using a coarser index of the distance from the niche maximum expected to show little sensitivity to uneven sampling effort across the total distribution area for species (details in Supplementary Methods 1).

Species-level changes and functional traits

To investigate potential ecophysiological mechanisms underlying the species-level variability in the post-1984 change of survivorship through time, we used a modified version of model M4 only considering the 40 species with measured functional trait data (M6; Supplementary Table 4), instead of all 81 species. Model M6 allowed testing of whether the differences in both average mortality risk and the pace of risk change over time could be explained by species traits (model details in Supplementary Methods 1).

The functional traits were measured between July and September 2015 on 81 dominant, canopy trees in seven of the 24 plots (Supplementary Table 7; Supplementary Tables 1, 2 for plots and species with trait data). For each plot, species were chosen with the aim of sampling those that made up 80% of the standing biomass for the most recent census. The details of trait data collection and measurements are presented in Bauman et al.[24] and are summarized here. Measured traits and their functions are presented in Supplementary Table 3 and Extended Data Fig. 5. The traits were measured on three individuals per species, and included leaf photosynthesis and stomatal conductance at a reference CO_2 concentration of 400 µmol mol^{-1} and irradiance of 1,500 µmol photons m^{-2} s^{-1} (Asat and gsat, respectively), dark respiration (Rd) at the same CO_2 concentration, the CO_2-saturated photosynthesis and stomatal conductance (Amax and gmax, respectively), measured at 1,200 µmol mol^{-1} CO_2. Estimates of leaf maximum carboxylation rate (Vcmax) and maximum light-driven electron flux (Jmax) normalized to 25 °C were obtained from the photosynthesis model found in ref. [78] fitted to the A–c_i curves (‘plantecophys’ R package[79]). The one-point method[80] was used to estimate Vcmax for each individual from net photosynthesis measured at 400 µmol mol^{-1} CO_2, and Jmax from net photosynthesis measured at 1,200 µmol mol^{-1} CO_2 (ref. [81]). We also measured leaf area, leaf mass per area, leaf thickness, wood density (from branches, after bark removal), leaf nutrient concentrations and stable carbon isotope ratio ($\delta^{13}C$). All traits were averaged at the species level for the analyses.

Sensitivity analyses for the risk trend

We ran four sensitivity analyses to test the robustness of the temporal trend in mortality risk increase after removing major influences of wind damage-related disturbances from cyclones. To do so, we created two subsets of the initial raw survival dataset by filtering out (1) any census interval affected by a cyclone (see black triangles in Fig. 1b), or (2) any plot having had at least one cyclone disturbance, even minor, since 1971. The resulting datasets had, respectively, 23 and five plots, and 69 and 15 species presenting over 400 observations. We generated the latent survival probabilities per stem per year (*K*_lat) for each species separately, on the basis of these two datasets (see eq. 1), and ran models M3 and M4 to test for plot-level and species-level temporal trends in mortality risk. All four resulting sensitivity analyses indicated that the mortality risk trend remained clear across plots and species, even after removing the main impact of major wind-related disturbances (Extended Data Fig. 4, Supplementary Table 6).

Modelling climate over time

To explore the implications of the differences in mortality risk with long-term mean climate and the position of species on their climatic niche, we built a separate set of models to investigate temporal trends in *T*max, VPD and MCWD from 1971 to 2019. To do so, we used Bayesian generalized additive models, modelled the monthly values of the three climate variables separately with B-splines and a maximum of four basis functions to constrain the wiggliness of the relation[82], and added varying intercepts for the different plots. The resulting trends indicated a strong increase of *T*max and VPD over time across all plots (consistent with results from Bauman et al.[24]), but no directional increase in MCWD (Fig. 1c, Extended Data Fig. 11).

Bayesian updating of the parameters

The parameter probability posteriors of the size-dependent survival models were fitted separately for each species in Stan, using the No-U-Turn-Sampler (NUTS; 5,000 iterations on three chains), with the ‘rstan’ R package[83]. For the models M1 and M3 to M6, Bayesian updating of the parameter probability distributions were fitted with the NUTS in Stan, by running 6,000 iterations on four chains, with 1,000 ‘warmup’ steps, using the R package ‘brms’[84] (R code in Supplementary Methods 2). Chain convergence was checked through Rhat values, ensuring that they were all within 0.01 from 1, and mixing of all chains was assessed visually. Coefficient posteriors were summarized through their median and 95% HPDI (that is, the narrowest posterior interval encompassing 95% of the probability mass, corresponding to the coefficient values most consistent with the data[82]). Model covariates were considered important when their coefficient 95% HPDI did not encompass zero, indicating a strong-enough level of confidence to report the effect as positive or negative. All analyses were carried out in the R statistical environment[85] with the R code available in Supplementary Methods 2.

Reporting summary

Further information on research design is available in the Nature Research Reporting Summary linked to this paper.

Data availability

The raw demographic data that supported the findings are available in Bradford et al.[58], in the CSIRO Data Access Portal (https://doi.org/10.4225/08/59475c67be7a4). The survival dataset used for the 81 studied species was archived on the platform of the Terrestrial Ecosystem Research Network infrastructure (https://doi.org/10.25901/rxtc-th28), which is enabled by the Australian Government’s National Collaborative Research Infrastructure Strategy. The climate data used in the models are openly available under the same DOI, and trait data will be made available on reasonable request.

Code availability

A detailed and commented R code supporting the findings of this study is available in Supplementary Methods 2 as well as on the same Terrestrial Ecosystem Research Network repository as the data (https://doi.org/10.25901/rxtc-th28).

58. Bradford, M. G., Murphy, H. T., Ford, A. J., Hogan, D. L. & Metcalfe, D. J. Long-term stem inventory data from tropical rain forest plots in Australia. *Ecology* **95**, 2362 (2014).
59. Johnson, D. J. et al. Climate sensitive size-dependent survival in tropical trees. *Nat. Ecol. Evol.* **2**, 1436–1442 (2018).
60. Needham, J., Merow, C., Chang-Yang, C.-H., Caswell, H. & McMahon, S. M. Inferring forest fate from demographic data: from vital rates to population dynamic models. *Proc. Biol. Sci.* **285**, 20172050 (2018).
61. Lewis, S. L. et al. Tropical forest tree mortality, recruitment and turnover rates: calculation, interpretation and comparison when census intervals vary. *J. Ecol.* **92**, 929–944 (2004).
62. Reeves, J., Chen, J., Wang, X. L., Lund, R. & Lu, Q. Q. A review and comparison of changepoint detection techniques for climate data. *J. Appl. Meteorol. Climatol.* **46**, 900–915 (2007).
63. Clark, J. S., Bell, D. M., Kwit, M. C. & Zhu, K. Competition-interaction landscapes for the joint response of forests to climate change. *Glob. Chang. Biol.* **20**, 1979–1991 (2014).
64. Oliva, J., Stenlid, J. & Martínez-Vilalta, J. The effect of fungal pathogens on the water and carbon economy of trees: implications for drought-induced mortality. *New Phytol.* **203**, 1028–1035 (2014).
65. Franklin, J. F., Shugart, H. H. & Harmon, M. E. Tree death as an ecological process. *Bioscience* **37**, 550–556 (1987).
66. Yanoviak, S. P. et al. Lightning is a major cause of large tree mortality in a lowland neotropical forest. *New Phytol.* **225**, 1936–1944 (2020).
67. Preisler, Y., Tatarinov, F., Grünzweig, J. M. & Yakir, D. Seeking the ‘point of no return’ in the sequence of events leading to mortality of mature trees. *Plant Cell Environ.* **44**, 1315–1328 (2020).

68. Aragão, L. E. O. C. et al. Spatial patterns and fire response of recent Amazonian droughts. *Geophys. Res. Lett.* **34**, L07701 (2007).
69. Malhi, Y. et al. The linkages between photosynthesis, productivity, growth and biomass in lowland Amazonian forests. *Glob. Chang. Biol.* **21**, 2283–2295 (2015).
70. Hutchinson, M. F., Xu, T., Kesteven, J. L., Marang, I. J. & Evans, B. J.ANUClimate v2.0, NCI Australia. https://doi.org/10.25914/60a10aa56dd1b (2021).
71. Abatzoglou, J. T., Dobrowski, S. Z., Parks, S. A. & Hegewisch, K. C. TerraClimate, a high-resolution global dataset of monthly climate and climatic water balance from 1958–2015. *Sci. Data* **5**, 170191 (2018).
72. Carscadden, K. A. et al. Niche breadth: causes and consequences for ecology, evolution, and conservation. *Q. Rev. Biol.* **95**, 179–214 (2020).
73. Swenson, N. G. et al. A reframing of trait–demographic rate analyses for ecology and evolutionary biology. *Int. J. Plant Sci.* **181**, 33–43 (2020).
74. Morueta-Holme, N. et al. Habitat area and climate stability determine geographical variation in plant species range sizes. *Ecol. Lett.* **16**, 1446–1454 (2013).
75. Brum, M. et al. Hydrological niche segregation defines forest structure and drought tolerance strategies in a seasonal Amazon forest. *J. Ecol.* **107**, 318–333 (2019).
76. Chitra-Tarak, R. et al. The roots of the drought: hydrology and water uptake strategies mediate forest-wide demographic response to precipitation. *J. Ecol.* **106**, 1495–1507 (2018).
77. Boria, R. A., Olson, L. E., Goodman, S. M. & Anderson, R. P. Spatial filtering to reduce sampling bias can improve the performance of ecological niche models. *Ecol. Modell.* **275**, 73–77 (2014).
78. Farquhar, G. D., von Caemmerer, S. & Berry, J. A. A biochemical model of photosynthetic CO_2 assimilation in leaves of C3 species. *Planta* **149**, 78–90 (1980).
79. Duursma, R. A. Plantecophys—an R package for analysing and modelling leaf gas exchange data. *PLoS ONE* **10**, e0143346 (2015).
80. De Kauwe, M. G. et al. A test of the 'one-point method' for estimating maximum carboxylation capacity from field-measured, light-saturated photosynthesis. *New Phytol.* **210**, 1130–1144 (2016).
81. Bloomfield, K. J. et al. The validity of optimal leaf traits modelled on environmental conditions. *New Phytol.* **221**, 1409–1423 (2019).
82. McElreath, R. *Statistical Rethinking: A Bayesian Course with Examples in R and STAN* (CRC Press, 2020).
83. "RStan: the R interface to Stan." R package version 2.21.2. http://mc-stan.org/ (Stan Development Team, 2020).
84. Bürkner, P.-C. brms: An R package for Bayesian multilevel models using Stan. *J. Stat. Softw.* **80**, 1–28 (2017).
85. R Core Team. R: a language and environment for statistical computing. https://www.R-project.org/ (R Foundation for Statistical Computing, 2021).
86. Dinerstein, E. et al. An ecoregion-based approach to protecting half the terrestrial realm. *Bioscience* **67**, 534–545 (2017).

Acknowledgements We thank A. Cheesman for his help with field work in Bellenden Ker, and M. Torrello Raventos for the first census of Bellender Ker. D.B. was funded by the Belgian American Educational Foundation (BAEF), the Philippe Wiener–Maurice Anspach Foundation, and the European Union's Horizon 2020 research and innovation programme under the Marie Skłodowska-Curie grant agreement no. 895799. G.D. was supported by the Philippe Wiener–Maurice Anspach Foundation. Y.M. was supported by the Frank Jackson Foundation. S.M.M. was partially funded by NASA grant 20-CARBON20-0033. J.A.-G. was funded by the UK Natural Environmental Research Council (NERC; grants NE/T011084/1 and NE/S011811/1). The trait campaign and data analysis were funded by NERC grant NE/P001092/1 to Y.M. and the European Research Council projects T-FORCES (Tropical Forests in the Changing Earth System; 291585) to O.L.P. and Y.M., and GEM-TRAIT (321131) to Y.M., under the European Union's Seventh Framework Programme (FP7/2007-2013). We acknowledge the foresight of G. Stocker in establishing the CSIRO permanent plots and the many CSIRO staff and volunteers who have helped to measure and maintain the plots since 1971; thankful to the Daintree Rainforest Observatory for providing a subsidy on accommodation and station fees, and to the Australian Supersite Network, part of the Australian Government's Terrestrial Ecosystem Network (Daintree Rainforest, Cow Bay, and Robson Creek Supersites) for provision of data used as part of the study. Computational resources have been provided by the Consortium des Équipements de Calcul Intensif (CÉCI), funded by the Fonds de la Recherche Scientifique de Belgique (F.R.S.-FNRS) under grant no. 2.5020.11 and by the Walloon Region. This study is a product of the Global Ecosystems Monitoring (GEM) network.

Author contributions D.B. and S.M.M. designed the study and the statistical models of tree survival. D.B. tidied and vetted the demographic and trait data and performed the analyses. D.B. led the writing with regular feedback from S.M.M., Y.M. and C.F. on intermediate stages of the analyses and manuscript. G.D. extracted species biographical data and the climatology associated with their locations to calculate species climatic niches. S.W.R. helped to generate the climatic covariates. L.A.C. and L.P.B. led the trait data collection, assisted by R.D., B.E.M., H.R.N.-R., J.R.C.P. and P.E.S.-A. and initiated and supported by Y.M. M.F.H. provided the raw climate product from ANUClimate. M.B. supplied demographic data for the 20 CSIRO plots and Robson Creek. C.F., L.A.C., S.W.R., J.A.-G. J and G.D. provided feedback on the discussion. S.G.W.L. contributed demographic data of the Daintree Observatory and commented on the manuscript. All authors commented on the manuscript and gave their approval for publication.

Competing interests The authors declare no competing interests.

Additional information

Supplementary information The online version contains supplementary material available at https://doi.org/10.1038/s41586-022-04737-7.

Correspondence and requests for materials should be addressed to David Bauman.

Peer review information *Nature* thanks Maxime Cailleret, Brendan Choat and Xiangtao Xu for their contribution to the peer review of this work. Peer reviewer reports are available.

Reprints and permissions information is available at http://www.nature.com/reprints.

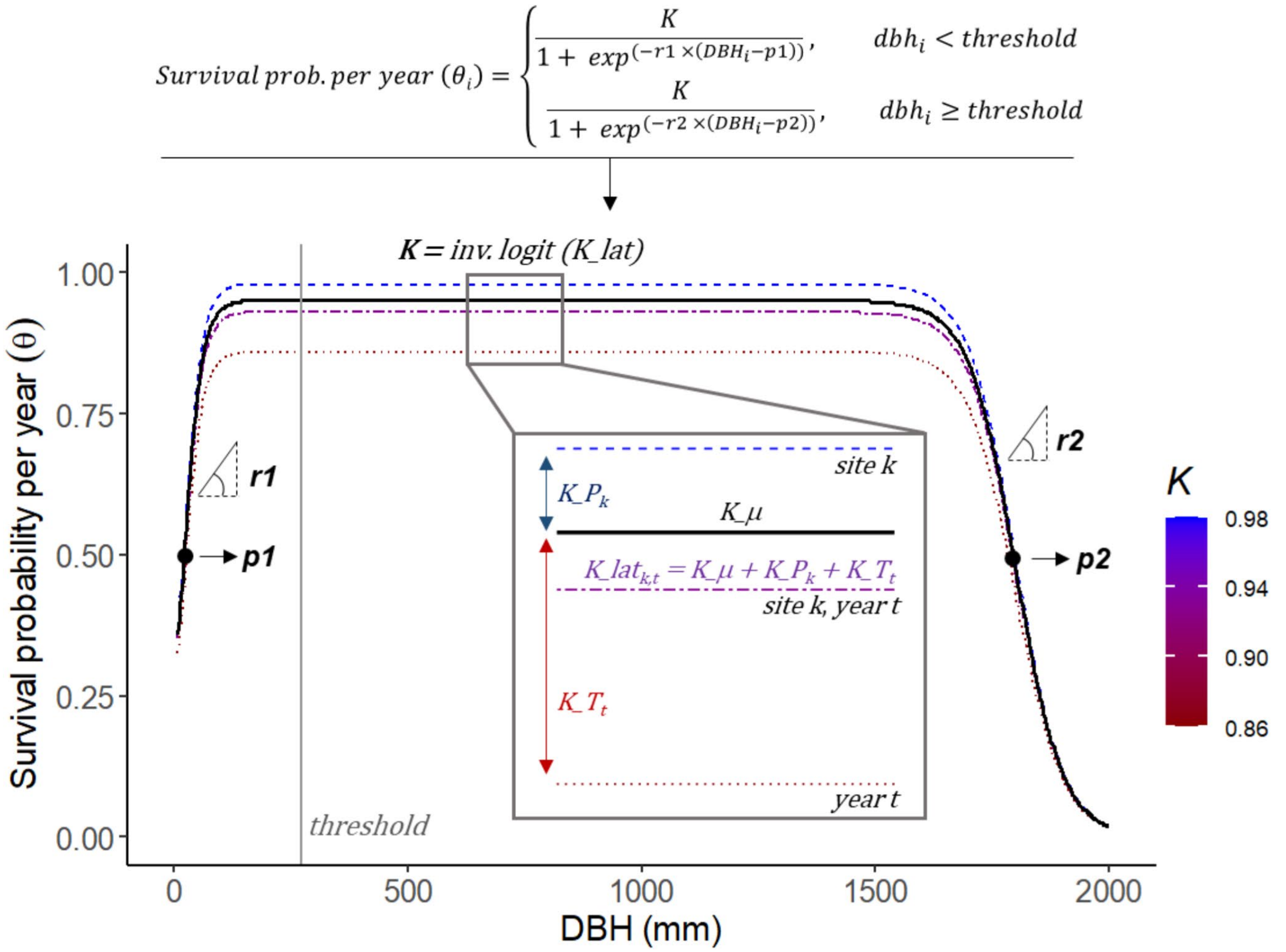

$$Survival\ prob.\ per\ year\ (\theta_i) = \begin{cases} \dfrac{K}{1 + exp^{(-r1 \times (DBH_i - p1))}}, & dbh_i < threshold \\ \dfrac{K}{1 + exp^{(-r2 \times (DBH_i - p2))}}, & dbh_i \geq threshold \end{cases}$$

Extended Data Fig. 1 | Schematic illustration of the size-dependent multilevel survival model and its parameters. Survival probability per year (theta) for a given species is defined by either one of two similar logistic functions, depending on a DBH threshold, only changing in the sign of *r* (*r1* > 0, *r2* < 0), yielding two S-shaped logistic function related through their common plateau *K*. This size-dependent model of survivorship was fitted separately for each of the 81 studied species. *p1* and *p2* are the inflection points of the two curves, with *p2* characterising the species DBH at 50% survival per year. *r1* and *r2* are rates of survival change per year in the corresponding portions of the survival curve. While *K* was initially the background survival rate of the species during most of the tree live[59,60], our model decomposes *K* into a species-specific average survival rate per year across all the sites and years (*K_μ*), a site-specific deviation from the average (*K_P*), a year-specific deviation from the average (*K_T*), and an error term (not represented, here). Because nearly all species occurred in multiple plots, and because different plots were recensused on different years, every two to five years mostly, the overlap of census years across plots allowed us to infer a latent survival probability per year, between 1971 and 2019 (*K_lat*). *K_lat*, the latent logit-survival probability per year, generated separately for each species through this survival model, was used as the response variable of all subsequent analyses (M1 to M6, see Supplementary Table 4) to study how species' mortality risk (i.e. 1 - survivorship, or 1 - *K*) changed through the years, whether this change varied among species and sites, and how climate, species' climatic niche, and species functional traits related to mortality risk changes through time. Examples of the above theoretical curve from some of the studied species are presented in Extended Data Fig. 2.

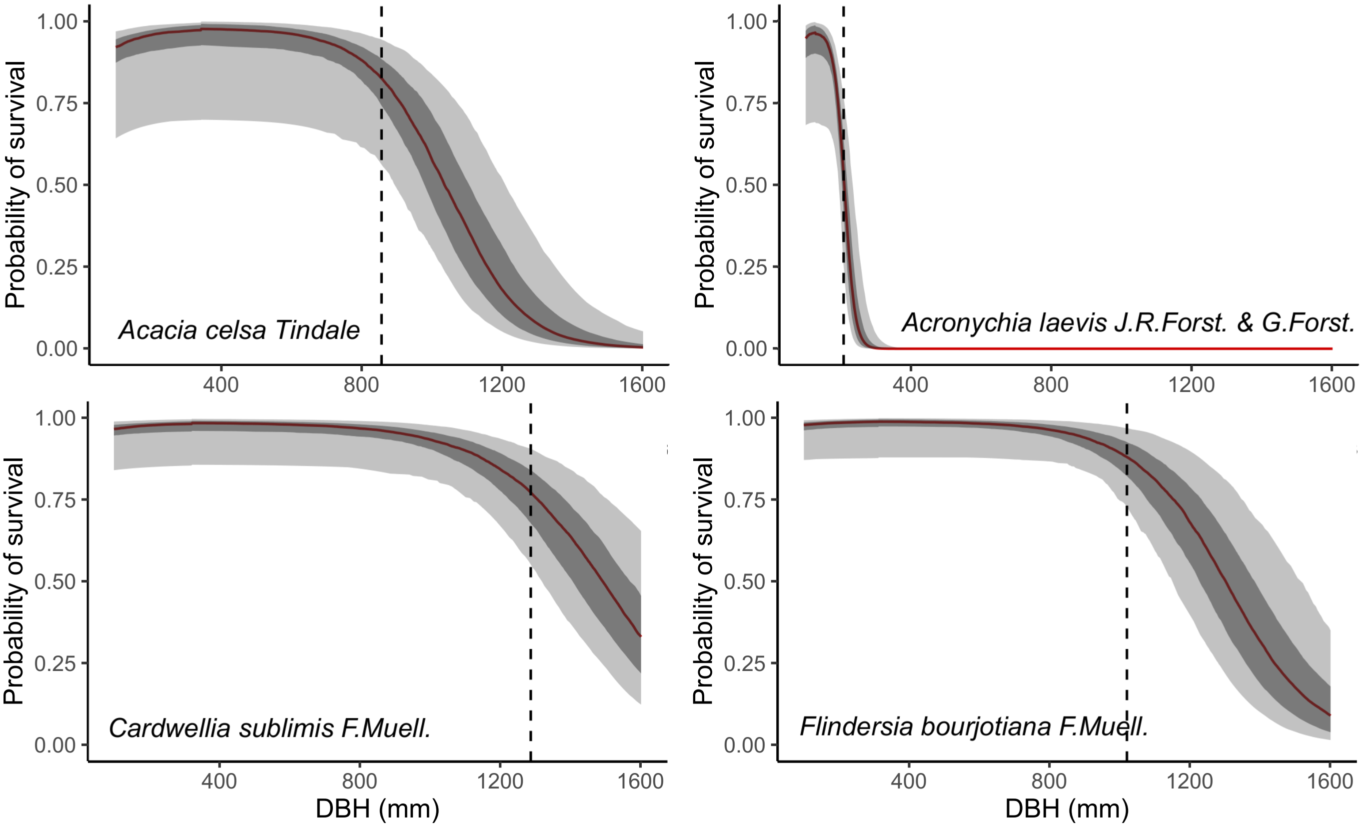

Extended Data Fig. 2 | Illustration of the interspecific variability of survival probability as a function of tree diameter. The figures represent species-specific survival probability predictions between 10 and 160 cm DBH for four of the 80 species of the study, across forest plots and years, based on the species-specific Bayesian multilevel models of survival (eq. 1; Extended Data Fig. 1). The red line is the posterior survival probability per year median, and the dark and light grey shaded areas are the 50%- and 90% posterior credibility intervals, respectively. Vertical dashed lines correspond to the observed maximum DBH for the corresponding species (*Acacia celsa Tindale*, *Acronychia laevis J.G.Forest & G.Forst*, *Cardwellia sublimis F.Muell.*, and *Flindersia bourjotiana F.Muell.*).

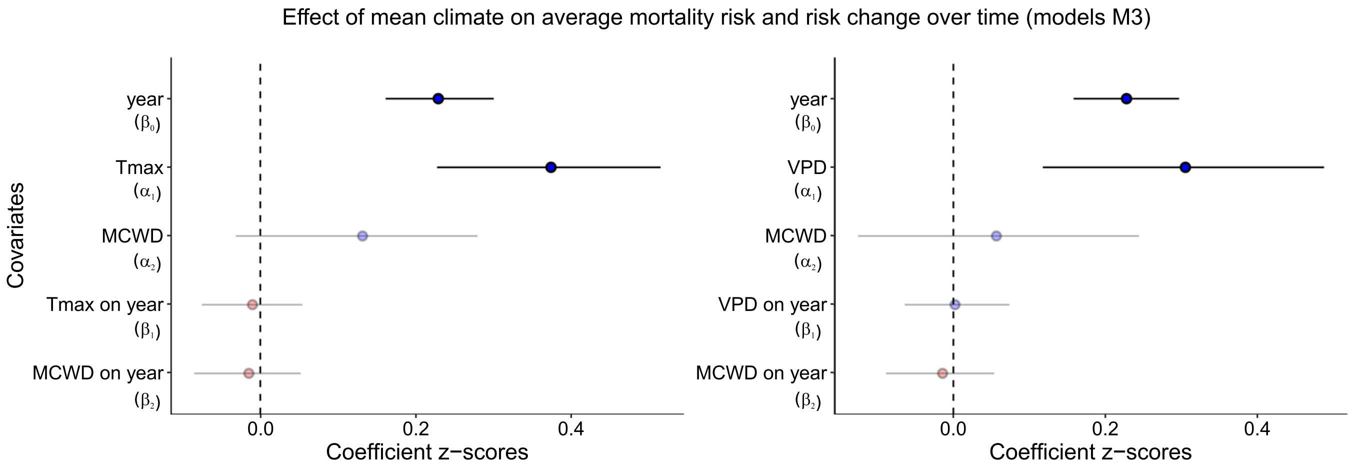

Extended Data Fig. 3 | Effects of local climate on average mortality risk and mortality risk temporal change across plots (models M3). Model M3 tests the effect of 'year', and either Tmax and MCWD, or VPD and MCWD on mortality risk (see es. 3; Tmax and VPD tested in separate models to limit collinearity, see Supplementary Methods 1). Climate variables influence the model grand intercept (average mortality risk across plots, α_0) and grand 'year' slope (mortality risk increase over time, β_0), through coefficients $\alpha_{1\text{-}2}$ and $\beta_{1\text{-}2}$, respectively. Average mortality risk is higher in plots presenting on higher long-term mean monthly Tmax and VPD during the warmest/driest quarter (95%-HPDI of α_1 encompass positive values only). Mean climate does not clearly predict how steep the temporal increase in mortality risk is among the plots (95%-HPDI encompass zero).

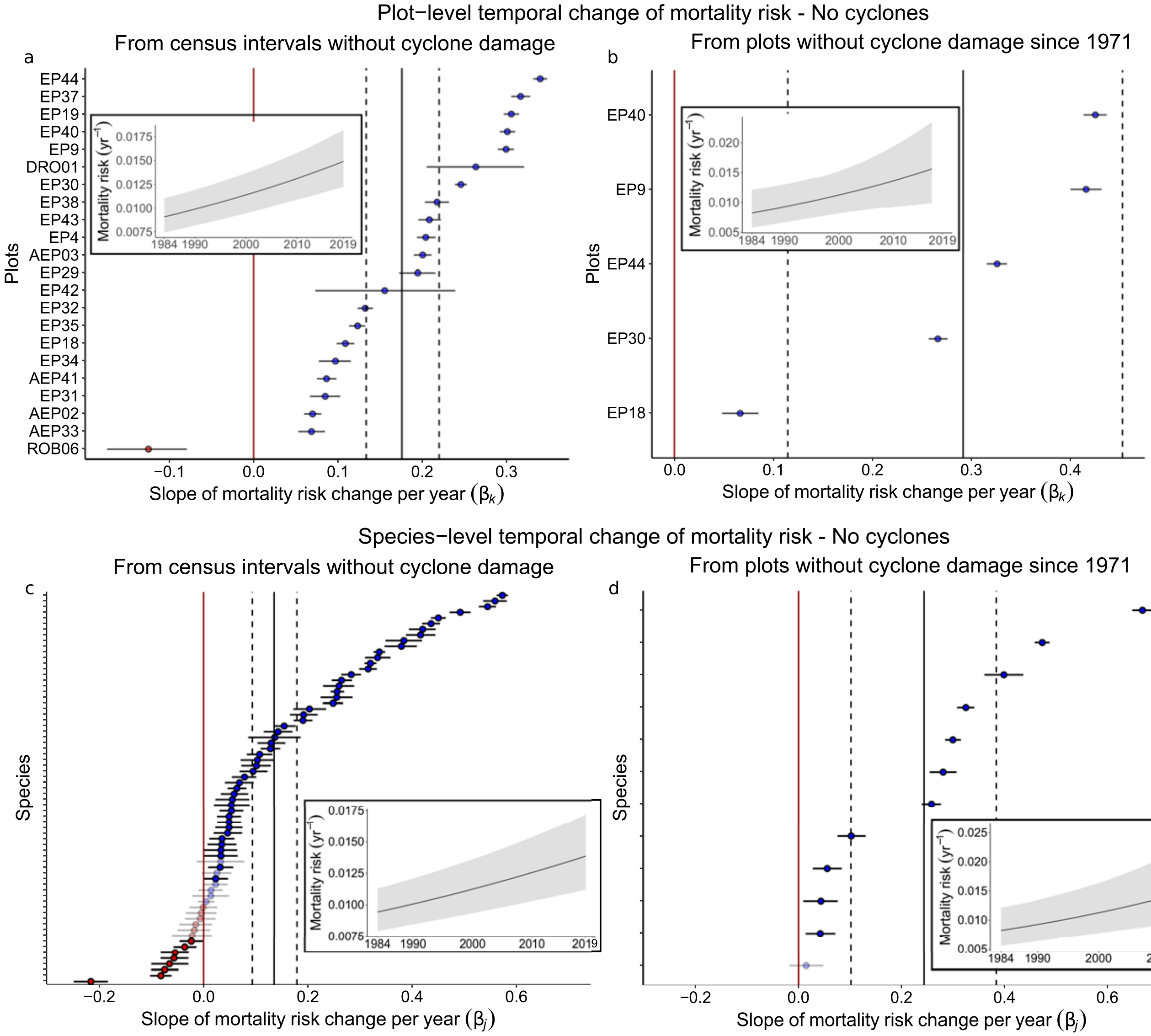

Extended Data Fig. 4 | Sensitivity analyses of the mortality risk increase over time: Species-level and plot-level slopes of change of mortality risk per year (1984-2019) without influence of cyclones. **a**, **c**, Plot-level (**a**) and species-level (**c**) slopes of mortality risk change per year (β_k and β_j, respectively; eqs. 3 and 4), obtained with models M3 and M4 on the basis of the subset of survival data obtained from the first approach to remove the effect of cyclones: Any census interval in a plot damaged by a cyclone was removed from the initial dataset, and the Bayesian size-dependent survival model (eq. 1) was run for the species that presented >400 observations in the reduced dataset. Models M3 and M4 were then run on the resulting latent survival probabilities *K_lat* (see eqs. 1, 3, 4) to test for temporal changes in mortality risk across plots and species, with plot-level and species-level slopes. **b**, **d**, The second approach to remove the influence of cyclones consisted of only keeping the plots that remained totally unaffected by cyclones in the last 49 years (see Supplementary Methods 1), then selecting the species that had >400 observations in the remaining plots, generating the latent survival probability per year (*K_lat*; eq. 1), and running models M3 and M4 as for the first approach. **a**–**d**, Species and plots whose 95%-highest posterior density interval (HPDI) encompassed zero are half-transparent. Blue and red circles indicate clear mortality increase and decrease through time, respectively (intervals not encompassing zero). The black vertical solid and dashed lines are the median and 95%-HPDI of the grand 'year' slope (i.e. generalisable effect across plots (**a**, **b**) and species (**c**, **d**)). The two approaches to test the robustness of the mortality risk temporal change without the main influence of cyclones (removal of intervals, or removal of plots) respectively had 69 and 15 species, and 23 and five plots The percentage and number of plots and species whose mortality risk increased between 1984 and 2019 for approach 1 and 2 respectively were 96% (22) and 100% (5) of the plots, and 81% (56) and 92% (11) of species.

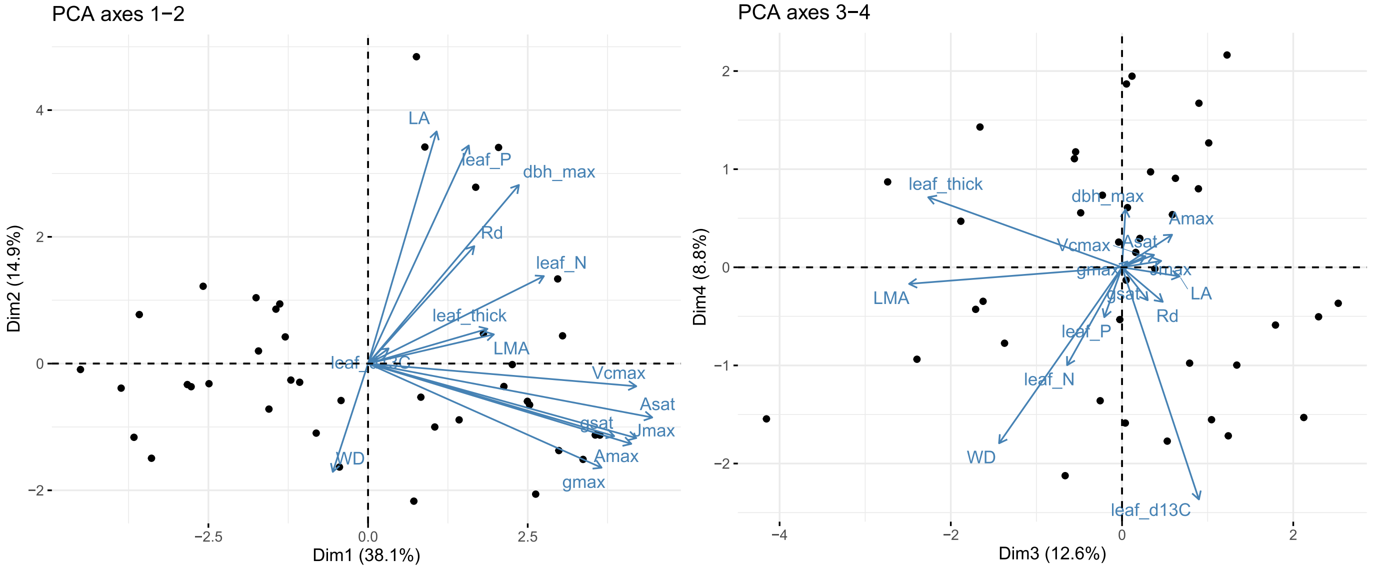

Extended Data Fig. 5 | Illustration of functional trait relationships among the 40 species with trait data, used in the M6 models of mortality risk over time. The figures represent the functional space occupied by the 40 tree species on the first four ordination axes of a correlation PCA, together describing 71.4% of the trait values (see Supplementary Table 3 for trait abbreviations).

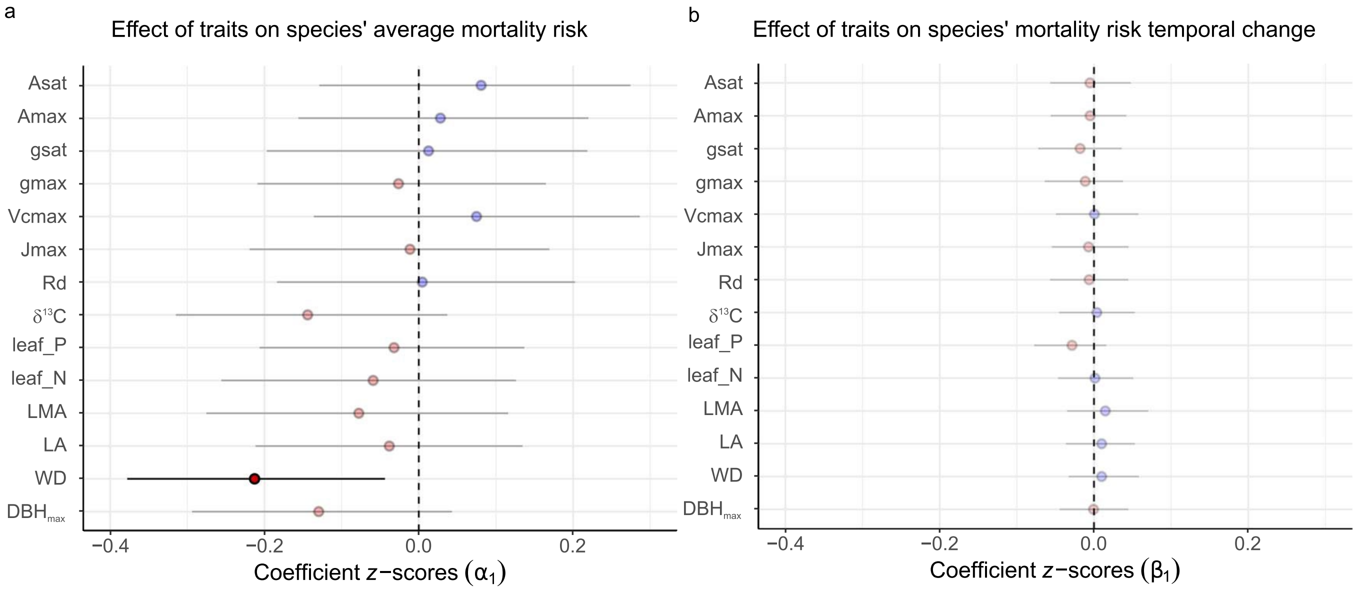

Extended Data Fig. 6 | Effects of species functional traits on average mortality risk and mortality risk change through time. a, **b**, Trait mediation of species-level intercept and 'year' slopes (α_1 and β_1, respectively, see eqs. 6 in Supplementary Methods 1). **a**, Positive and negative slopes indicate traits increasing and decreasing average mortality risk, respectively. **b**, Positive slopes correspond to traits that accentuate the rate of mortality risk change per year, while negative slopes correspond to attenuations of this rate. Circles and intervals are median and 95%-highest posterior density intervals (HPDI) for slope coefficients α_1 (trait effect on average mortality risk) and β_1 (trait mediation of 'year' effect on mortality risk) (see eq. 6).

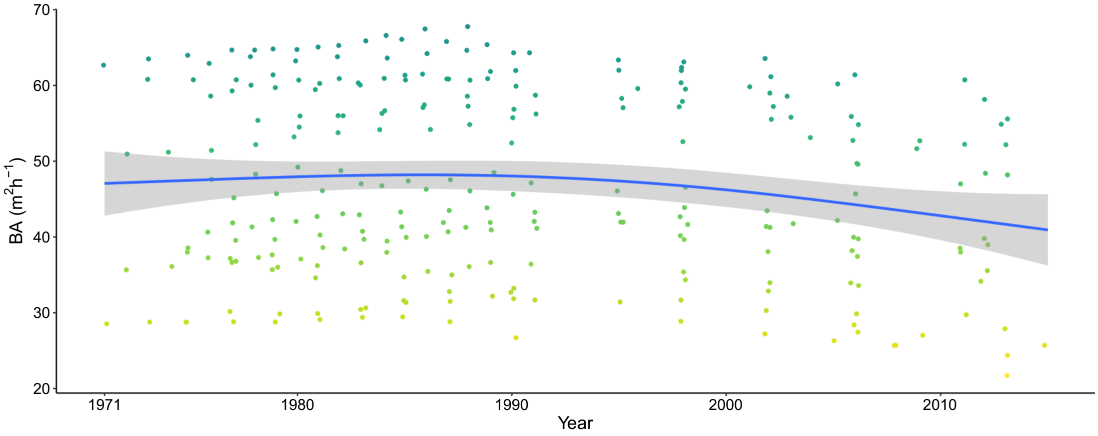

Extended Data Fig. 7 | Change of stand-level basal area per hectare (BA) over time. Change of BA per forest plot between 1971 and 2019 (a). Each circle is a plot BA on the year beginning a census period. The smooth curve and shaded area are the mean and 95% confidence interval of a generalised additive model (GAM), showing a decrease in plot BA across plots, and within most plots. The circle colour is proportional to the BA value (yellow to blue for low to high BA).

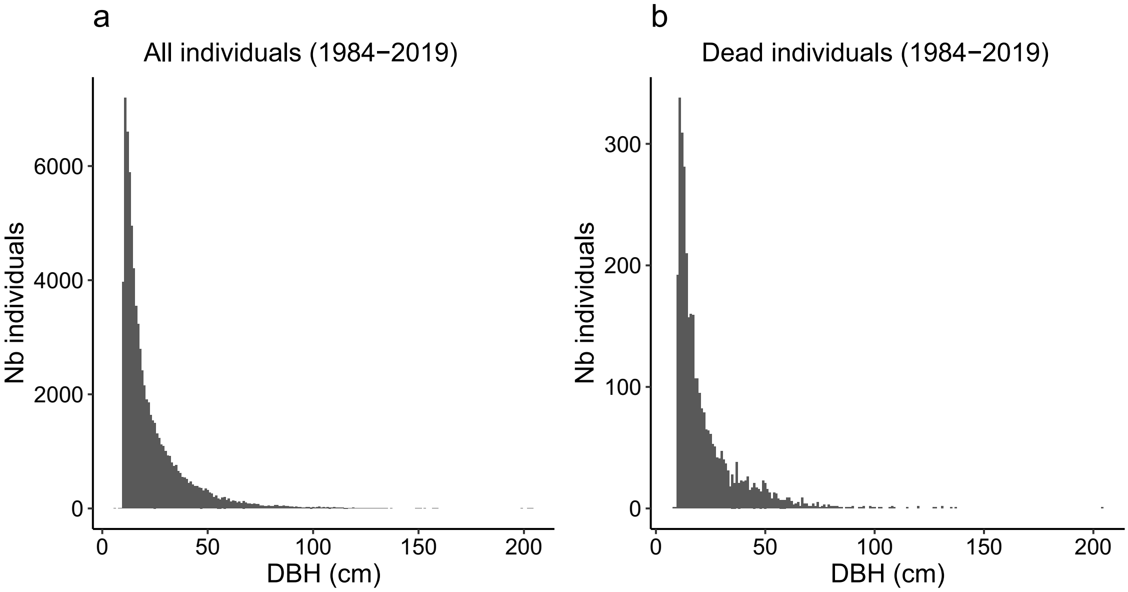

Extended Data Fig. 8 | Living and dead tree DBH distributions for the time period 1984-2019. The histogram bins are 1 cm-wide. We explored the relation between increased mortality risk and tree DBH visually and did not detect any clear size association. A Pearson's Chi-squared test with simulated p-value confirmed that no clear link could be detected between the proportions of alive and dead individuals in DBH bins of 1 or 5 cm (Chi-squared$_{bin\_5cm}$ = 0.0054, p-value = 1).

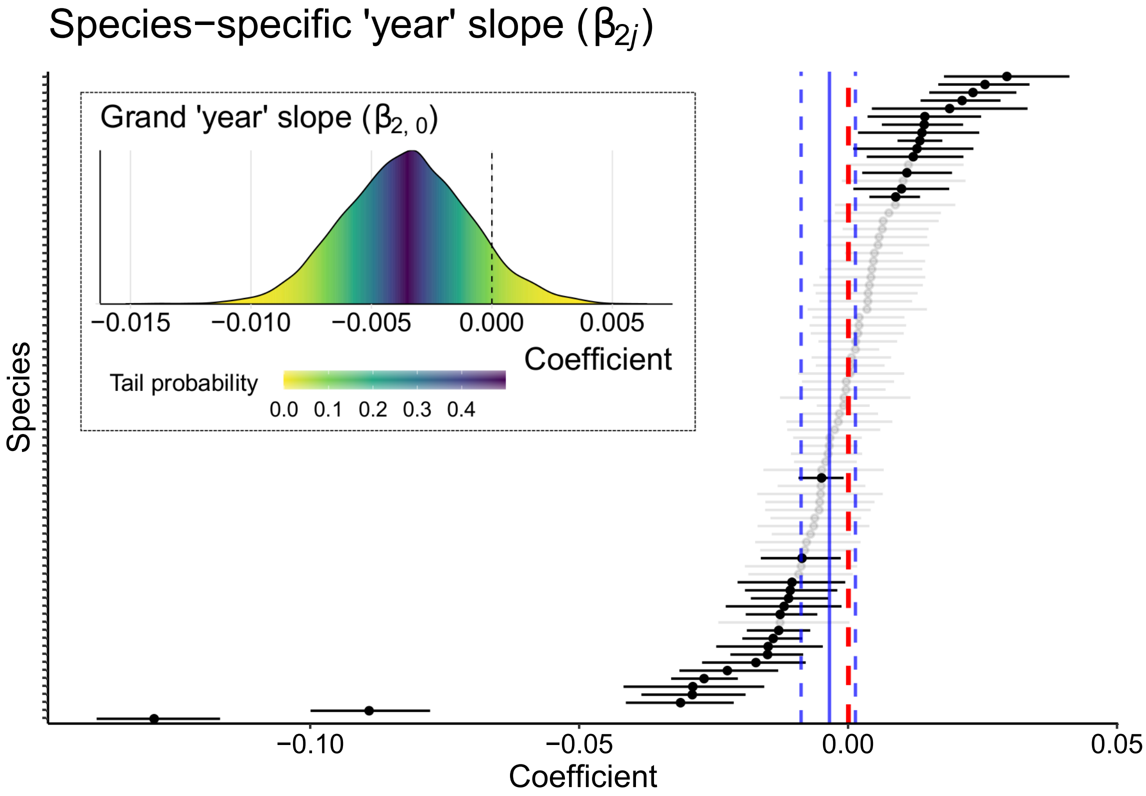

Extended Data Fig. 9 | Changes of log-transformed absolute diameter growth rate (AGR) over time across and within species, for the 81 studied species. The main figure shows the species-level coefficients of AGR change per year, between 1971 and 2019 (species-specific 'year' slope; β_{2j} in eqs. 7, Supplementary Methods 1). Circles and horizontal bars are posterior median and 95% highest posterior density intervals (HPDI). Plain black circles and bars are species whose posterior 95%-HPDI did not encompass zero; semi-transparent circles and bars are species whose HPDI encompassed zero (no clear AGR increase or decrease). The red dashed line marks zero, that is, the separation between coefficient values indicating an increase of AGR over time (positive values) and a decrease of AGR over time (negative values). The vertical plain and dashed blue lines are the median and 95%-HPDI of the grand year slope (see inset). The inset shows the posterior probability distribution of the coefficient of AGR change per year across all species (i.e. grand 'year' slope mean; $\beta_{2,0}$ in eqs. 7, Supplementary Methods 1). Overall, AGR did not clearly increase or decrease across species (unlike mortality risk; Fig. 3). AGR increased for 14 species and decreased for 19 species, while remaining mostly unchanged (95%-HPDI encompassing zero) for 48 species (semi-transparent circles and horizontal bars).

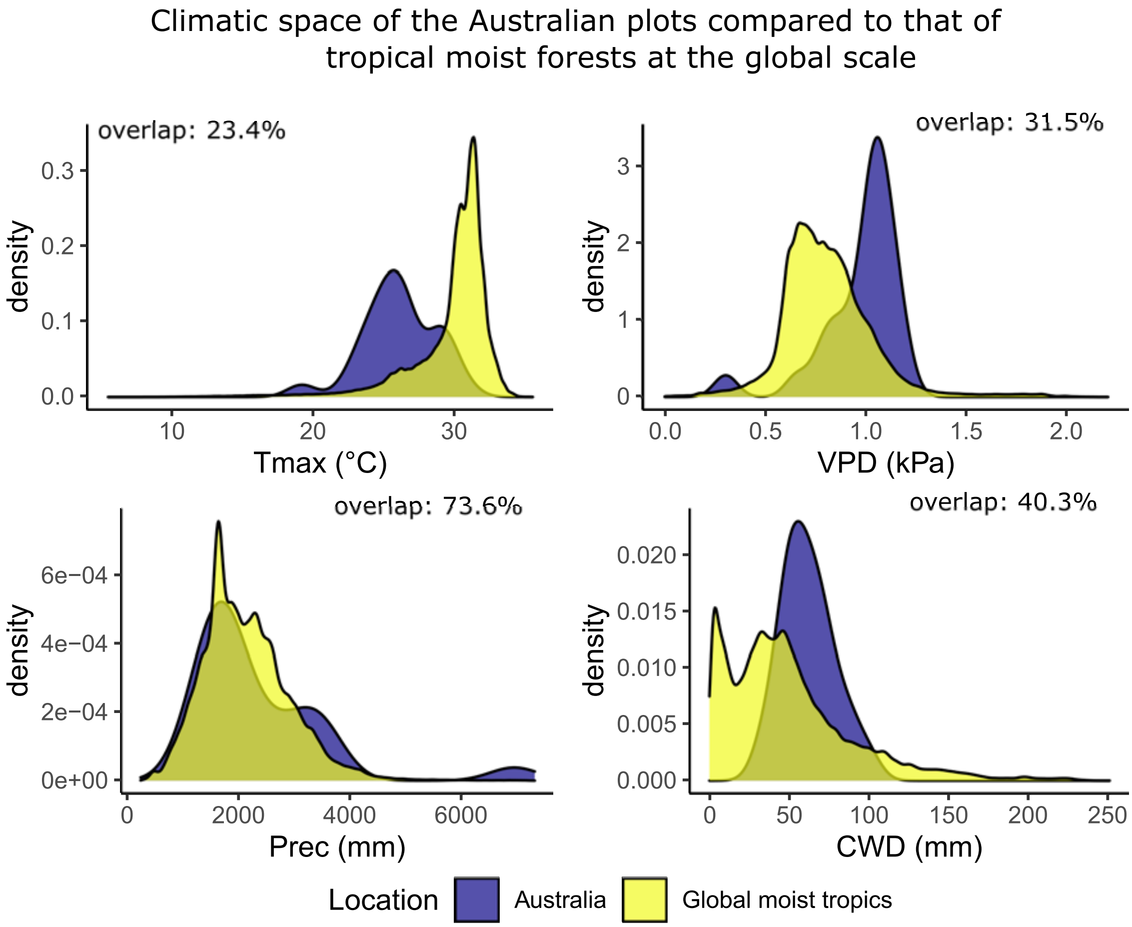

Extended Data Fig. 10 | Comparison of the climatic space occupied by the 24 plots of Australian tropical moist forests of the study with the total climatic space of tropical moist forests worldwide. The climatic spaces were obtained from 30-year climate averages (1981-2010) extracted from TerraClimate[71], combined with the spatial locations of the grid cells belonging to the biomes “Tropical and subtropical moist broadleaf forests” (including tropical montane forests)[86] (see https://ecoregions2017.appspot.com/).

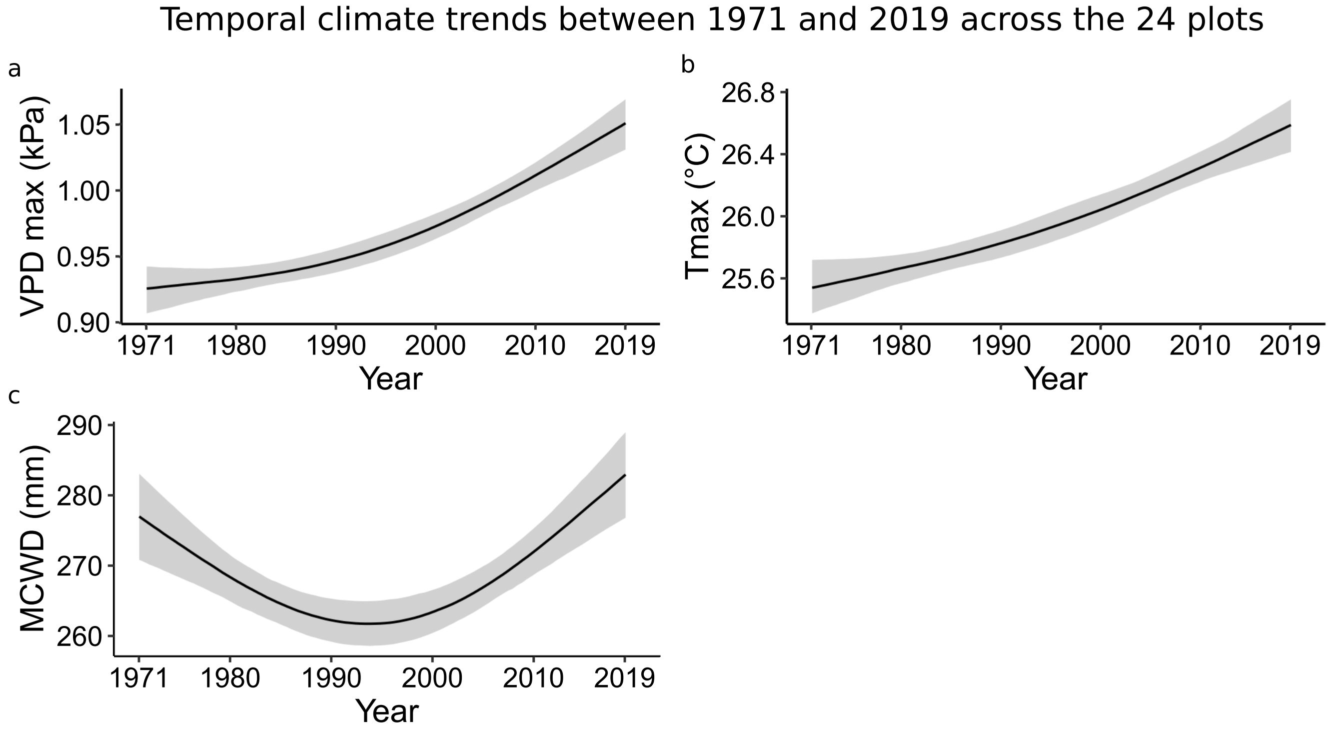

Extended Data Fig. 11 | Overall temporal trends in climate across the environmental gradient. Three Bayesian B-spline models with varying plot intercept and four basis functions were used to model monthly VPD, Tmax and MCWD over time across all 24 plots (see Methods). Both temperature and VPD showed a strong increase across all plots. MCWD did not show any clear directional trend across plots (more details in ref. [24].